



**COMPUTATIONAL FLUID DYNAMICS SIMULATION OF A PROTON
EXCHANGE MEMBRANE ELECTROLYZER**

Lappeenranta–Lahti University of Technology LUT

Master's programme in Energy Conversion, Master's thesis

2023

Henri Hovinen

Examiners: Professor, Teemu Turunen-Saaresti

Marta Zocca, D.Sc. (Tech.)

ABSTRACT

Lappeenranta–Lahti University of Technology LUT

LUT School of Energy Systems

Energy Technology

Henri Hovinen

Computational fluid dynamics simulation of a proton exchange membrane electrolyzer

Master's thesis

2023

75 pages, 34 figures, and 8 tables

Examiners: Professor Teemu Turunen-Saaresti and Marta Zocca, D.Sc. (Tech.)

Keywords: CFD, Electrolysis, PEM-Electrolyzer, Simulation, Hydrogen production

The transition of the global energy sector from fossil fuels towards renewable-based energy systems necessitates development of methods and technologies to perform as energy storages and produce energy carrier mediums. Hydrogen in particular has been discussed as a potential energy carrier medium, which is produced by electrolyzers, devices which dissect water into their atom components of hydrogen and oxygen. The design of electrolysis devices often requires careful planning in the design phase, as the costs of the technology can be quite severe for the emerging technology. The design can be assisted with computational fluid dynamics, which has also developed new methods for electrolysis simulation in the recent years.

This master's thesis investigated academic literature for recent methods, simplifications and developments of electrolyzer simulations in academic circles. Based on the observations made during the literature review, a three-dimensional straight channel proton exchange membrane electrolyzer was simulated using the commercial ANSYS® package. The results of the simulations were compared against measured performance data and were discovered to be in good agreement. Current density distribution in the electrolyzer cell was studied across three select voltages of 1,535 V, 1,656 V, and 1,746 V, alongside flow velocity patterns, hydrogen volume fraction patterns and effects turbulence. Additionally, the effect of increasing and decreasing the thickness of the membrane of the electrolyzer cell was studied. It was discovered that reducing the membrane thickness from 50 μm to 30 μm increased the performance of the cell, with a voltage of 1,702 V producing current density value of 1,03 A/cm^2 for the 30 μm thick membrane, whereas the 50 μm thick membrane cell produced current density value of 0,82 A/cm^2 .

TIIVISTELMÄ

Lappeenrannan–Lahden teknillinen yliopisto LUT

LUTin energijärjestelmien tiedekunta

Energiatekniikka

Henri Hovinen

Protoninvaihtokalvo-elektrolysaattorin laskennallinen virtaussimulaatio

Energiatekniikan diplomityö

2023

75 sivua, 34 kuvaa ja 8 taulukkoa

Tarkastajat: Professori Teemu Turunen-Saaresti ja Marta Zocca, D.Sc. (Tech.)

Avainsanat: CFD, Elektrolyysi, PEM-Elektrolysaattori, Simulaatio, Vedyntuotanto

Globaalin energiasektorin siirtymä fossiilisten polttoaineiden käytöstä uusiutuviin energialähteisiin vaatii uusien teknologioiden ja metodien kehittämistä, jotka voivat toimia energiavarastoina ja sekundaaristen energialähteiden tuottajina. Puheenaiheena on ollut erityisesti vety, jota tuotetaan elektrolysaattorilla jakamalla vesimolekyylit niiden atomikomponentteihin: vetyyn ja happeen. Elektrolysaattorilaitteiden rakentaminen vaatii usein tarkkaa ja huolellista arviointia suunnitteluvaiheessa, koska tuoreen teknologian kustannukset voivat olla suuret. Laitteen suunnittelua voi avittaa laskennallisella virtausmekaniikalla, johon on myös kehitetty lähivuosina uusia metodeja elektrolyysin mallintamiseen.

Tässä diplomityössä tutkittiin akateemisessa kirjallisuudessa elektrolyysin mallintamiseen käytettyjä metodeja, yksinkertaistuksia ja kehityksiä. Kirjallisuuskatsauksesta poimitujen havaintojen avulla muodostettiin kolmiulotteinen laskennallinen virtaussimulaatio protoninvaihtokalvo-elektrolysaattorista suorilla virtauskanavilla käyttäen kaupallista ANSYS®-ohjelmistopakettia. Simulaation tuloksia verrattiin mitattuun suorituskykydataan, joiden todettiin olevan hyvässä linjassa tulosten kanssa. Virrantiheyttä tutkittiin kolmessa valitussa jännitteessä, jotka olivat 1,535 V, 1,656 V, and 1,746 V. Virrantiheyden lisäksi samoissa jännitteissä tutkittiin virtausnopeuden kuvioita, vedyn tilavuusosuuksia, ja turbulenssin mallintamisen vaikutusta. Lisäksi työssä tutkittiin kalvonpaksuuden muutoksen vaikutusta elektrolysaattorin toimintaan. Tulosten perusteella kalvon paksuuden laskeminen 50 μm :sta 30 μm :n kasvatti laitteen suorituskykyä: 1,702 V:n jännitteellä simulaatio tuotti 1,03 A/cm^2 virrantiheyden arvon 30 μm paksulla kalvolla, kun taas vastaavalla jännitteellä simulaatio tuotti 0,82 A/cm^2 virrantiheyden alkuperäisellä 50 μm paksulla kalvolla.

ACKNOWLEDGEMENTS

This master's thesis has been done in a partial co-operation with my employer Etteplan Oyj, where I was provided with an academic licence for ANSYS® software and hardware to perform the simulations made for the thesis. I would like to thank my supervisor Kati for allowing me to use my workplace resources to write my thesis and allowing me to flexibly adjust my time for work, this thesis, and finishing the rest of my remaining studies. I would also like to thank everyone from the fluid dynamics team at Etteplan, for taking me under their wing and helping me learn new things about CFD every single day.

With the formalities out of the way, I would like to thank all of my fellow student friends, with whom I have spent countless days and hours trying to somehow reach this point in our studies. In no particular order, thank you Niko, the other Niko, Sampo, Juho, Vilho, Totte and Jere. Many curse words, laughs and frustrations were displayed during these five years, and that made my studies something I will remember and cherish for the rest of my life.

I would also like to thank Professor Teemu Turunen-Saaresti and Marta Zocca for guiding me throughout this thesis. Special thanks to Teemu for suggesting the topic of this thesis to begin with and giving great insights and suggestions for me during the thesis. Marta deserves a special mention as well, for despite her being on parental leave at the time, she still somehow found time and wanted to listen to my problems with the thesis work and gave great suggestions for solving said problems.

I would also like to thank my family, who despite the distance between us and at worst seeing each other only twice or thrice per year always offered their support whenever I needed it. The greatest thanks however must go to my significant other, Veera, who always offered her full support no matter how insignificant the problem or issue was, whether it was studies-related, or life-related in general. She made me laugh and smile, and life in Lappeenranta would have been grimmer indeed without her.

Henri Emil Hovinen

Tampere, 26.11.2023

SYMBOLS AND ABBREVIATIONS

Roman characters

A	area	[m ²]
c	concentration	[mol/m ³]
d	diameter	[m]
E	activation energy	[J/mol]
EW	equivalent weight	[kg]
G_R	Gibbs free energy	[kJ/mol]
H_R	reaction enthalpy	[kJ/mol]
\vec{i}	ionic current density	[A/m ³]
J	current density	[A/cm ²]
K	permeability	[m ²]
k	heat transfer coefficient	[W/mK]
L	length	[m]
M	molar mass	[g/mol]
\dot{n}	molar flow rate	[mol/s]
P	electrical power	[W]
p	pressure	[bar, MPa]
q_m	mass flow rate	[kg/s]
T	temperature	[°C, K]
U	voltage/potential	[V]
U_P	wetted perimeter	[m]
u	velocity	[m/s]

R_i	volumetric transfer current	[A/m ³]
S	reaction entropy	[J/K]
v	velocity	[m/s]
w	velocity	[m/s]

Greek characters

η_i	surface overpotential	[V]
ϕ	potential	[V]
μ	dynamic viscosity	[Ns/m ²]
ζ	specific active electrode surface area	[1/m ²]
σ	surface tension	[N/m]
ρ	density	[kg/m ³]
θ	contact angle	[deg]

Constants

F	Faraday constant	96,485 C/mol
R	ideal gas constant	8,314 J/kmol

Dimensionless quantities

α	charge transfer coefficient
γ	concentration dependence
γ_{er}	evaporation rate coefficient
γ_{cr}	condensation rate coefficient
γ_{ld}	liquid mass exchange rate constant
ε	porosity
η	efficiency
λ	water content

D_{gl}	diffusion coefficient
f_D	friction factor
n_d	osmotic drag coefficient
Re	Reynolds' number
s	liquid saturation
z	number of transferred electrons

Subscripts

a	anode side
c	cathode side
cell	electrolyzer cell
H ₂	hydrogen
H ₂ O	water
h	hydraulic
I	current based
in	inlet boundary
l	liquid phase
m	mixture phase
mem	membrane phase
O ₂	oxygen
op	operating conditions
out	outlet boundary
rev	reversible
sat	saturation
sol	solid phase

U voltage based

wv water as vapor

Superscripts

HHV high heating value

0 standard state conditions

ref reference value

Abbreviations

AEM Anion exchange membrane

CAD Computer assisted design

CL Catalyst layer

CFD Computational fluid dynamics

CPU Central processing unit

FEM Finite element method

GDL Gas diffusion layer

HHV Higher heating value

IEA International Energy Agency

PEM Proton exchange membrane or polymer electrolyte membrane

PtX Power-To-X

RSE Reynolds stress equation

SOE Solid oxide electrolysis

UDF User-defined function

Table of contents

Abstract	
Acknowledgements	
Symbols and abbreviations	
1 Introduction	10
2 Fundamentals and status of electrolysis modelling	14
2.1 Thermodynamics of electrolysis	15
2.2 Electrolysis technologies.....	18
2.2.1 Alkaline water electrolysis.....	18
2.2.2 Proton Exchange Membrane (PEM) electrolysis.....	22
2.2.3 Solid Oxide Electrolysis (SOE)	26
3 Modelling methodology	29
3.1 Computational fluid dynamics	30
3.1.1 Governing equations	31
3.1.2 Turbulence	32
3.1.3 Electrochemistry equations.....	32
3.2 Simulation workflow.....	38
3.2.1 Geometry description.....	40
3.2.2 Mesh.....	42
3.2.3 Solver settings and boundary conditions	46
4 Simulation results	52
4.1 Results with the “SIMPLE” scheme	55
4.2 Results with the “Coupled” scheme	58
5 Discussion of results.....	64
5.1 Best practices for electrolyzer simulations	68
6 Conclusions	72
References.....	75

1 Introduction

The global energy sector is currently undergoing a major transition caused by multiple factors, including increasing energy demand, climate change, and the political aspects and finite amount of fossil fuels. In Europe especially, the invasion of Ukraine by Russia has caused major disruptions to energy markets and has highlighted the instabilities provided by energy systems reliant on imported fossil fuels (IEA, 2023). The transition from fossil fuel-based energy systems to more renewables-based energy systems is also seen as a major pillar to reach the 1,5 °C target of the Paris agreement in 2015 to combat climate change.

As renewable energy sources such as wind and solar power have been estimated to reduce in their costs to the point of becoming the cheapest sources of energy in the future (IEA, 2022b), investments and research has been poured into combatting the variable nature of said energy sources. As the electricity demand will increase even further in the future as more and more systems and industries become electrified such as mobility by electric vehicles, the problem of storing renewable energy has become more relevant than ever before. This problem has been tackled with methods such as energy storage technologies and Power-To-X, or PtX, technologies. Common storage methods include batteries or pump facilities, where the excess electricity produced by renewable energy sources is stored and then discharged back into the electricity grid when conditions won't allow the full production of renewable energy to meet the electricity demand. An alternative method, PtX-technologies instead convert the excess electricity into different energy carrier mediums, such as gas, synthetic fuels, or hydrogen.

Hydrogen in particular has been emerging as a promising energy carrier medium. It is abundant, easily storable and moveable, and it can be used not only for electricity production, but also for refining metals such as steel, and as a fuel for hydrogen based electric vehicles. According to estimations made by International Energy Agency, or IEA (2022a), global installed hydrogen capacity can reach 134-240 GW in 2030. The primary method of converting excess renewable energy into hydrogen is done via electrolysis, where water molecules will be split into their hydrogen and oxygen components. This allows the production of so called "green hydrogen", where the whole energy production cycle produces net-zero carbon emissions. Hydrogen can be likewise converted back into

electricity with the usage of fuel cells, where the electrolysis process is reversed: hydrogen is combined with oxygen, which produces water molecules and energy. This has been illustrated in Figure 1:

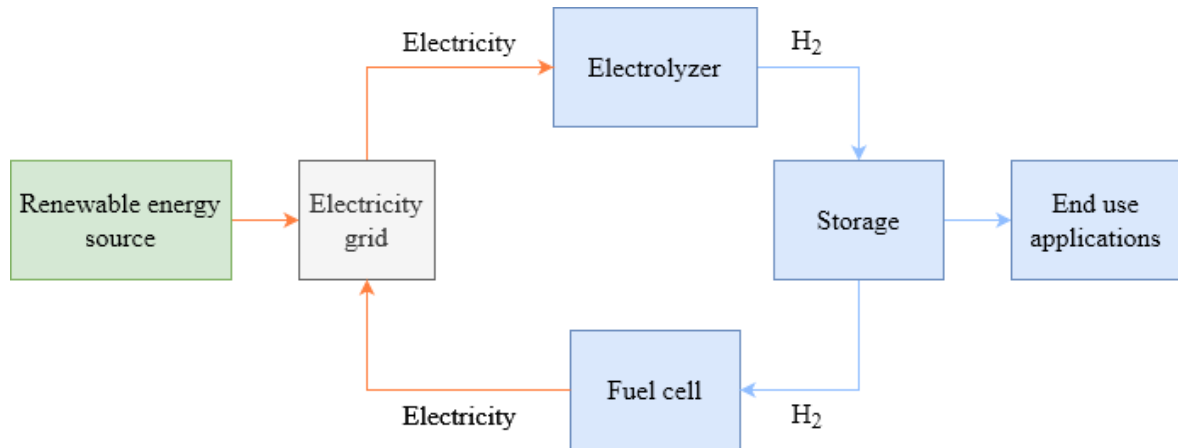


Figure 1. Basic cycle of hydrogen production in an energy system.

The design of electrolysis devices can be a daunting task, which requires keen understanding of the physics associated within the phenomena. This necessitates modelling and computational simulations to be used as tools for design. For this reason, the usage of Computational Fluid Dynamics, or CFD has steadily increased over the recent years to study electrolyzers.

As both computers and software have been developing side-by-side during the recent decades, the usage of CFD-based analysis for designing electrolyzer devices has become ever more cost-efficient and computationally efficient. The CFD method combines fluid dynamics with electrochemistry of electrolysis and allows the user to gain valuable information about the mass transfer, heat transfer and performance of the electrolysis device. Current commercially used and researched electrolysis methods include alkaline, proton exchange membrane (PEM), solid oxide (SOE), and anion exchange membrane (AEM) electrolysis. The most commercially used technologies of the four mentioned methods are the alkaline electrolysis and PEM-electrolysis (Bessarabov et al., 2015, p. 2-8) (Xiang et al., 2016), whereas the solid oxide and anion exchange membrane have only recently began emerging commercially, after many years of having only laboratory-scale applications. Figure 2 depicts search results for research articles featuring the words “modelling” and the corresponding electrolyzer type on ScienceDirect:

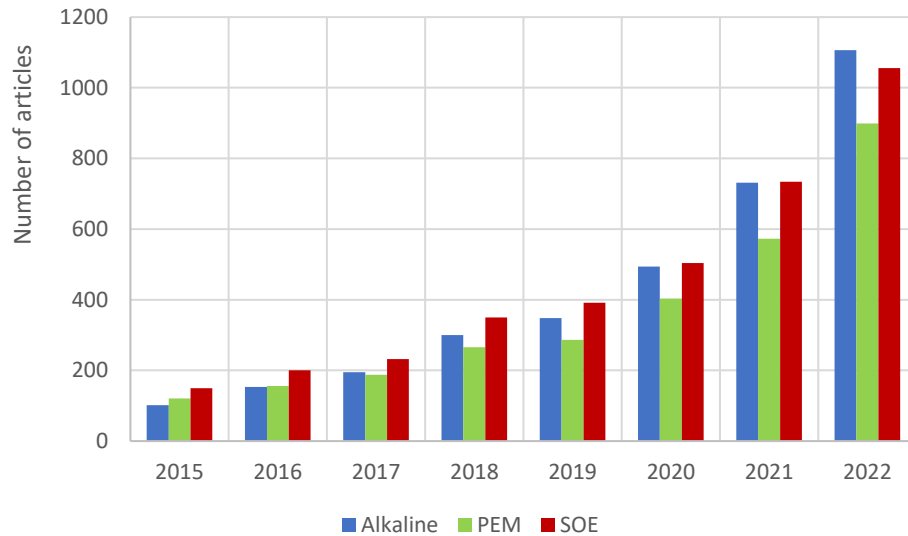


Figure 2. Search results for different electrolyzer types from ScienceDirect, data accessed on 03.07.2023.

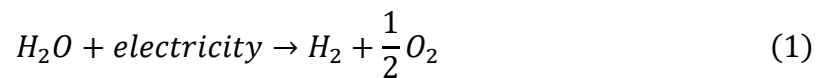
One can observe from the quick survey done that research towards electrolyzer modelling has been steadily increasing since 2015. An interesting development is the high number of articles about SOE electrolyzer modelling, despite its lack of major commercial use.

The main goals for this master's thesis can be depicted in two steps: First, scientific literature is to be investigated to discover the current status for electrolyzer numerical simulations in academic circles. Additionally, common validation methods and any simulation strategies performed in academic literature will be highlighted with great interest. The second major goal for the thesis is to simulate a three-dimensional proton exchange membrane-electrolyzer cell, with all associated physics. These include heat and mass transfer, charge transfer and electrochemistry. All simulations will be conducted with the commercial ANSYS® 2023R1 package with an academic license, which includes computer assisted design-, or "CAD", software for geometry definition, meshing software for grid generation, and solver software for both pre- and postprocessing of the simulation. The thesis will be structured as a guideline for future possible simulations. Therefore, an important subgoal of the thesis is to catalogue all best practices discovered during the development of the electrolyzer simulation. This includes possible mistakes made and how to avoid them, possible issues related to mesh generation, and any issues found out in the solver stage, whether on convergence or solution accuracy.

The thesis begins with a chapter of fundamental thermodynamic principles for electrolysis in general. Afterwards, the literature review on electrolysis CFD modelling is presented, alongside descriptions for the corresponding electrolysis technologies. The modelling methodology of the simulation segment of the thesis is divided into two subchapters, the first subchapter explains the theory behind the simulations, and the second subchapter explains the actual simulation development, which includes geometry, mesh, boundary conditions, etc. After the methodology, the results of the simulations are presented, and discussed. Finally, conclusions will be drawn on the simulation results, and the literature review to conclude the thesis.

2 Fundamentals and status of electrolysis modelling

Essentially, electrolysis is an electrochemical reaction in which water molecules will be dissected into their atom components: hydrogen and oxygen. This reaction is endothermic: it does not occur naturally. Thereby, the reaction requires external energy in order to function, which in the case of an electrolyzer is applied via electrical energy. The electrochemical reaction can be expressed simply as:



The application of the above-mentioned Equation 1 changes depending on the used electrolysis method.

Devices which utilize electrolysis in order to produce hydrogen are referred to as electrolyzers. Typically, electrolyzers consist of a cathode and an anode as the electrodes, electrolytes, catalysts, and membranes, diaphragms, or some other type of barriers between anode and cathode sides of the electrolyzer.

The electrodes are responsible for conducting the electricity current into the electrolyzer. The negative electrode is referred to as the cathode, and the positive electrode is referred to as the anode. At the anode side protons are separated from the water molecules with the oxidation reaction, which are then attracted by the negative cathode electrode where the positively charged protons recombine with negatively charged electrons forming pure hydrogen.

The electrolyte is the medium in the electrolyzer where the ions separated from the water molecules transfer towards the cathode side. This medium can be liquid or solid, depending on the electrolyzer type. In many cases, the medium is a type of caustic solution, especially when considering alkaline water electrolysis (Bessarabov et al., 2015, p. 3).

The catalysts are thin layers of a substance which enhances the rate of the reactions happening in the electrolyzer. Sometimes the catalysts are simple coatings on the electrodes, or sometimes they can be their separate layers. The catalysts require high reaction kinetic enhancing properties, alongside high durability since they tend to be placed in the electrolyte

solution. Materials which display such properties, such as platinum and iridium, are one of the main reasons electrolyzer costs have been so high. (Bessarabov et al., 2015, p. 5-6)

The barriers between anode and cathode side are used to prevent the produced hydrogen from recombining with oxygen and becoming water again. Likewise, the material of the barrier, whether it is a membrane, or a diaphragm is also a conducting component, as it also transports the ions from anode side to cathode side. In the case of membranes for example, the barrier is a thin, porous medium.

Modelling of electrolysis is challenging, as it encompasses and links the physics of electrochemistry, heat and mass transfer, and fluid dynamics. In order to begin the modelling process, one must first understand the basic thermodynamic principles of electrolysis.

2.1 Thermodynamics of electrolysis

The equations presented in this chapter are compiled and displayed as written by Bessarabov et al. (2015, p. 17-20, 22-23).

As previously mentioned, the electrolysis reaction is endothermic: deconstruction of water molecule into hydrogen and oxygen requires a specific amount of external energy. This amount of external energy required for the splitting of molecule bonds is referred to as reaction enthalpy, and can be written as an equation based on the first law of thermodynamics:

$$\Delta H_R = \Delta G_R + T\Delta S_R \quad (2)$$

Where ΔG_R is the required Gibbs free energy, and $T\Delta S_R$ is the entropy term representing the thermal input to the system. During standard state conditions, the Gibbs free energy is constant 236,483 kJ/mol.

With the Gibbs free energy, we can estimate the minimal electrical work needed to cause the molecular separation in water. This quantity is referred to as reversible cell potential, and can be written as:

$$U_{\text{rev}}^0 = \frac{\Delta G_R^0}{z \cdot F} \quad (3)$$

Where ΔG_R^0 is the free Gibbs energy during standard state conditions, which again, is 236,483 kJ/mol, z is the number of electrons transferred and F is the Faraday constant 96,485 C/mol. This would then give $U_{\text{rev}}^0 = 1,229$ V as the value of reversible cell potential.

However, since the external energy brought into the system in order to match the reaction enthalpy must be fully implemented with electrical energy, we can estimate the minimum reference voltage required for separating hydrogen and oxygen from each other during standard state conditions with the reaction enthalpy of water, Faraday constant and the number of electrons transferred during the reaction. This voltage is referred to as thermoneutral voltage:

$$U_{\text{th}}^0 = \frac{\Delta H_R^0}{z \cdot F} \quad (4)$$

Where ΔH_R^0 is the reaction enthalpy for water during standard state condition, which is 285,83 kJ/mol. The Equation (4) would then give us the minimal voltage needed for molecular separation of water without an external thermal source, which would be $U_{\text{th}}^0 = 1,481$ V.

It should be noted that the reaction enthalpy of electrolysis reaction is also a function of operating pressure, which affects the reversible cell potential. This can be illustrated with the Nernst equation, which links the electrode potential differences with concentrations of the reactant molecules. The equation can be written as:

$$U_{\text{rev}} = U_{\text{rev}}^0 - \frac{R \cdot T}{2 \cdot F} \cdot \ln \left(\frac{c_{\text{H}_2\text{O}}}{c_{\text{H}_2} \cdot c_{\text{O}_2}^{\frac{1}{2}}} \right) \quad (5)$$

Where U_{rev}^0 is the reversible cell potential during standard stat conditions [V], R is the ideal gas constant [8,314 J/kmol], F is the Faraday constant and $c_{\text{H}_2\text{O}}$, c_{H_2} , and $c_{\text{O}_2}^{\frac{1}{2}}$ are the concentrations of reactants [mol/m³]. If we substitute the concentrations with partial pressures of the reactants and include the operational pressure, we can change the Nernst equation to be written as:

$$U_{\text{rev}} = U_{\text{rev}}^0 - \frac{R \cdot T}{2 \cdot F} \cdot \ln \left(\frac{\frac{p_{\text{H}_2\text{O}}}{p_{\text{op}}}}{\left(\frac{p_{\text{H}_2}}{p_{\text{op}}}\right) \cdot \left(\frac{p_{\text{O}_2}}{p_{\text{op}}}\right)^{\frac{1}{2}}}\right) \quad (6)$$

The modified Nernst equation demonstrates how the reversible cell potential changes as the operational pressure or temperature are increased: it takes less voltage to cause water molecules to split into hydrogen and oxygen when the operational temperature is increased. Due to the logarithmic nature of the pressure term, there would be diminishing results in increasing the operational pressure.

The efficiency of a singular electrolysis cell can be defined with multiple different ways. For instance, one simple method is to define the efficiency with higher heating value, or HHV, molar flow rate of the produced hydrogen gas \dot{n}_{H_2} [mol/s], and with electrical power P [W] directed towards the electrolysis system:

$$\eta_{\text{cell}}^{\text{HHV}} = \frac{\text{HHV} \cdot \dot{n}_{\text{H}_2}}{P} = \frac{\text{HHV} \cdot \dot{n}_{\text{H}_2}}{U_{\text{cell}} \cdot I_{\text{cell}}} \quad (7)$$

Another method for defining the efficiency of a singular electrolysis cell is to use only the ratio of thermoneutral voltage and the actual cell voltage:

$$\eta_{\text{U}} = \frac{U_{\text{th}}^0}{U_{\text{op}}} \quad (8)$$

Where U_{th}^0 is the thermoneutral voltage during standard state conditions [V], see Equation (4), and U_{op} is the operational voltage of the electrolysis cell [V]. The accuracy of the voltage-based efficiency can be enhanced by considering the possible hydrogen losses caused by leaks and recombination of hydrogen and oxygen. This can be done with a separate current efficiency, which is the ratio of produced hydrogen and the theoretically produced maximum amount of hydrogen:

$$\eta_{\text{I}} = \frac{\dot{n}_{\text{H}_2}}{\dot{n}_{\text{H}_2, \text{theoretical}}}$$

The theoretical maximum amount of produced hydrogen can be expanded with Faraday's law; therefore, the current efficiency can be written as:

$$\eta_I = \frac{\dot{n}_{H_2}}{I_{\text{cell}} \cdot \left(\frac{1}{n \cdot F}\right)} \quad (9)$$

Where I_{cell} is the current of the cell [A], n is the amount of substance [mol], and F is the Faraday constant.

Now the efficiency of a singular electrolysis cell can be solved by taking the product of the voltage efficiency η_U from Equation 8 and the current efficiency η_I from Equation (9):

$$\eta_{\text{cell}} = \eta_U \cdot \eta_I \quad (10)$$

2.2 Electrolysis technologies

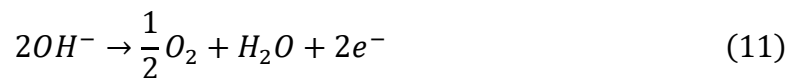
Stated as one of the main goals of the thesis, a literature review of the topic of modelling electrolyzers is conducted. The main sources of studies performed on the subject can typically be found from scientific magazines and published research papers.

Key aspects of the modelling studies from literature to be reviewed are the validation methods used to verify simulation results, information of the computational meshes, such as element size and count, what multiphase models are used, and computational loads and times used to reach converge in the simulations.

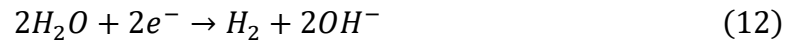
2.2.1 Alkaline water electrolysis

Alkaline water electrolysis utilizes potassium hydroxide KOH solution as its electrolyte. The electrodes are placed within the solution and are separated by a diaphragm to prevent the separated hydrogen and oxygen from combining again after the electrolysis reaction. The process has been depicted in Figure 3. The specific reactions which happen during alkaline water electrolysis can be written as:

For the anode:



And for the cathode:



Common operating conditions for an alkaline water electrolyzer range from 65 °C to 100 °C temperature-wise, and from 25-60 bar pressure-wise. (Bessarabov et al., 2015, p. 3-4)

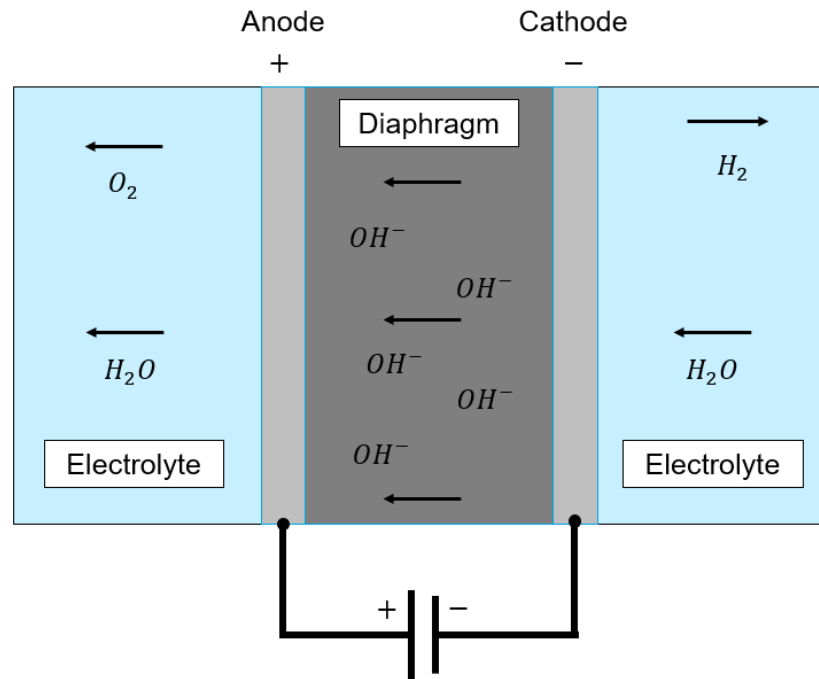


Figure 3. Basic process graphic of an alkaline water electrolyzer (Bessarabov et al., 2015, p. 3, modified from source)

Alkaline water electrolysis is considered to be the most mature of the electrolysis methods but suffers from a common problem newer application of CFD simulations have; there is not a significant amount of experimental and measurement data of hydrodynamics available on commercial scale electrolyzers (Wang et al., 2023) (Zarghami et al., 2020) (Lee et al., 2021). This makes validation of numerical simulations difficult, especially when considering studies on the hydrodynamics of the electrolyzer, such as the formation of the bubbles of hydrogen during production, or when developing new flow patterns. Nevertheless, as Figure 2 presents, there has been an increasing amount of research articles done on alkaline water electrolyzer modelling every year since 2015. Most of the articles instead use performance data to validate the numerical results.

Many of the recent numerical CFD studies of alkaline water electrolyzers are targeting the aforementioned bubble formation of hydrogen gas and the characteristics of multiphase flow in the electrolyzer (Zarghami et al., 2020) (Vachaparambil & Einarsrud, 2020) (Schillings et al. 2015). Another common aspect to study with CFD simulations is the flow pattern and development of more unorthodox flow channels to better combat the weaknesses of the alkaline water electrolyzer, which is the relatively limited current density when compared to other electrolyzer options (Wang et al., 2023) (Sandoval et al., 2021) (Rivera et al., 2021). According to Wang et al., this limited current density comes from the high overpotential of the electrolyzer, which leads to increased energy consumption. As commercial-scale alkaline water electrolyzers tend to be expensive to build, computationally costly, and complicated to set up properly, many studies have been simplified to consider smaller setups or 2D-domains, such as only the cathode flow channel side (Zarghami et al., 2020) (Lee et al., 2021) (El-Askary et al., 2015).

The research article written by Zarghami et al. (2020) featured a simplified 2D-computational domain of the cathode flow channel side. Instead of modelling the whole electrochemistry associated with electrolysis, the paper focused on the hydrodynamics of the electrolyzer: key phenomenon to study was the formation of the hydrogen bubbles in the cathode side. Instead of modelling the electrochemical reactions, this was conducted by implementing a mass source in the electrode side of the flow channel. The paper also conducted a study on the effect of turbulence model choice in the results. According to the authors, user-defined functions, or UDFs, for turbulent dispersion and drag forces were necessary to implement in order to reach more accurate results. The multiphase model used in the simulation was the Eulerian multiphase model, and ANSYS® Fluent 2019 R1 was used as the solver software. The research article does not disclose the computational time spent to reach convergence. An interesting find of the paper is the mention from the authors where commonly used turbulence models $k-\varepsilon$ and $k-\omega$ yielded surprisingly inaccurate results when compared to the chosen Reynolds stress equation, or RSE, -turbulence model. The results were validated and compared against experimental data provided by Riegel (et al., 1998), and were discovered to become more accurate the more active electrodes were implemented in the model. This phenomenon also occurred with higher values of current density. The authors theorized that some of the inaccuracies of the model could have come from slight momentum imbalance, which was further aggravated with the usage of the aforementioned $k-\varepsilon$ and $k-\omega$ turbulence models.

An example of a multidimensional alkaline water electrolyzer CFD simulation, a research article written by Lee et al. (2021) featured a model which included both anode and cathode sides. This included both flow channels, and current collectors alongside a separator. The authors also modelled the electrochemistry of electrolysis, utilizing UDFs which included equations for species conservation, source terms representing the consumption of said species due to the electrochemical reactions, and charge conservation. According to the paper, the key assumptions and simplifications of the model were laminar flow, transfer of small hydrogen and oxygen bubbles, negligible crossover of hydrogen and oxygen through the diaphragm isotropic porous electrode, and no inclusion of heat transfer. The main objective of the CFD study was the multidimensional model itself, and its validation through experimental data. Key output parameters were the distribution of the species concentration, current density and temperature. Instead of utilizing a multiphase model, the model solves its hydrogen transfer volume fractions with the aforementioned UDF-implemented species conservation equations. The authors used ANSYS® Fluent 2019 R2 as their solver and did not disclose the number of iterations or solver runtime when convergence was reached. The results of the multidimensional electrolyzer simulation were compared to experimental data (Schalenbach et al., 2016), and were found to reach similar patterns. A common validation method is the comparison of polarization curves, where the voltage of the electrolyzer is displayed as a function of current density. This comparison was performed for the research article, where the authors discovered that the CFD model provided satisfactory accuracy when compared to experimental data; the most discrepancy between the simulation and experimental data was discovered to happen at the lowest and highest values of current density. Other key observations were made when assessing the evolution reactions of hydrogen and oxygen: the largest rates of evolution reactions were found at the interfaces of the flow channels and the separator diaphragm. The article concluded by declaring that further studies to operating conditions and parameter optimization were necessary to develop the model further.

In conclusion, there is not a singular modelling method which dominates the modelling of alkaline water electrolysis. ANSYS® Fluent has been a common software, either with or without UDFs, but other software used for alkaline water electrolysis include MATLAB® and COMSOL® Multiphysics (Vera et al., 2011). Simulations range from simplified two-dimensional models with manually implemented mass sources to simulate bubble flow to more complex multidimensional cases with fully implemented electrochemistry equations

via UDFs. Validation methods have been almost universally the comparison of polarization curves, which is a common performance figure in electrolyzer industry. Researchers have found success in modelling alkaline water electrolysis with adequately accurate results with varying methods, with usually the most discrepancies between simulated and measured data come at very low or high values of current density, which might be due to the simplifications and assumptions such as neglect of heat transfer in the studies.

2.2.2 Proton Exchange Membrane (PEM) electrolysis

The PEM-electrolyzer utilizes a thin polymer membrane as the electrolyte to transport and conduct ions from the anode to cathode. The membrane also works similar to the diaphragm from an alkaline electrolyzer, as it also separates the oxygen and hydrogen gases after the electrolysis reaction. The specific reactions used in PEM-electrolysis can be depicted as:

For the anode:



And for the cathode:



Depicted in Equation (13), the water entering the electrolyzer is oxidized at the anode, which separates the hydrogen protons. These protons are then transported to the cathode side through the porous membrane in the middle of the electrolyzer, where they combine with the electrons in order to form pure gaseous hydrogen. Typical operating conditions of PEM-electrolyzers range from 50 °C to 80 °C temperature-wise, and from 8 bar to 85 bar pressure-wise. (Xiang et al., 2016) (Bessarabov et al., 2015, p. 5)

The basic structure of a PEM-electrolyzer has been depicted in Figure 4:

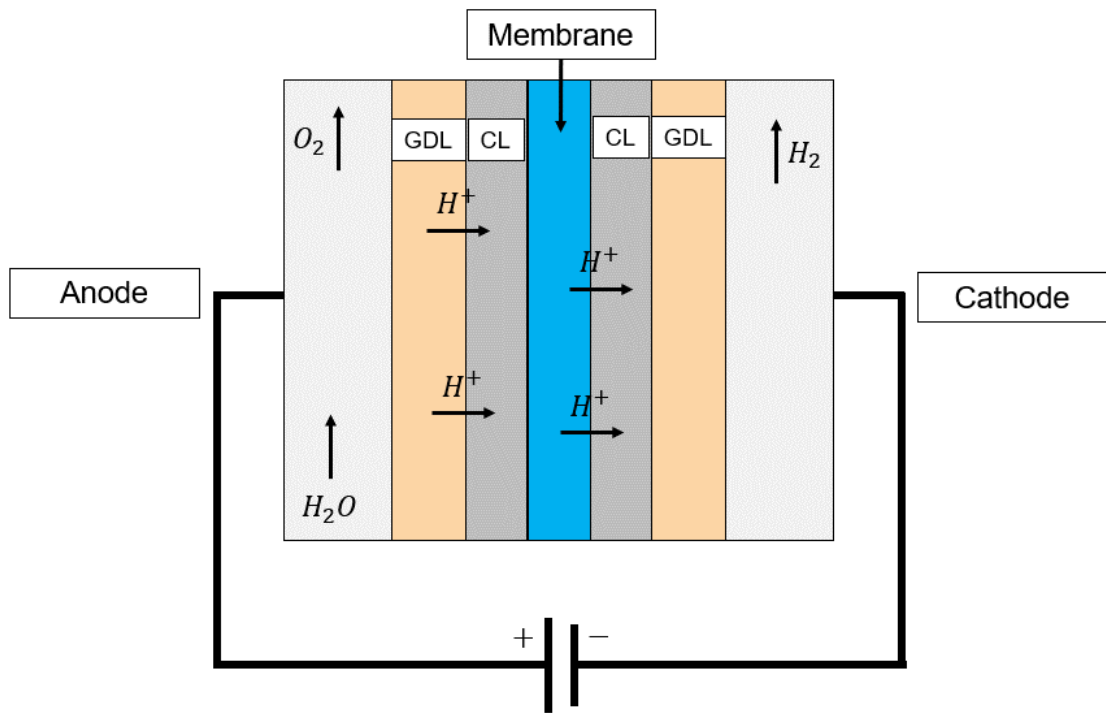


Figure 4. Basic process figure for PEM electrolyzer (Bessarabov et al., 2015, p. 14, modified from source). GDL stands for gas diffusion layer, and CL stands for catalyst layer.

Even though PEM-electrolysis is considered to be less mature a technology than alkaline water electrolysis, research interest for the technology has been steadily increasing every year since 2015, see Figure 2. As PEM-electrolyzers don't require a caustic aqueous solution as electrolyte, it is considered a safer option for hydrogen production. Additionally, PEM-electrolysis offers higher efficiency, and high current densities. The main weakness of the electrolysis method is its requirement for noble metals as catalysts and bipolar plates, which raise the costs of the electrolyzer significantly. Therefore, research towards the PEM-electrolysis modelling is targeting ways to minimize costs, and provide long-term operational capabilities (Zhang & Xing, 2020). It should also be noted that PEM electrolyzers have all the same components as proton exchange fuel cells have, which links research done on fuel cell modelling to electrolysis modelling (Chen et al., 2020). Essentially, the only major difference in modelling between a PEM- fuel cell and a PEM-

electrolyzer is the electrical potential: in a fuel cell, the electrical potential is zero on the anode side, whereas in an electrolyzer the electrical potential is zero on the cathode side.

A research paper written by Zhang & Xing (2020) featured a multidimensional CFD simulation of a PEM-electrolyzer. The model was built upon a geometry similar to Figure 4 with bipolar plates included at the anode and cathode sides. The authors modelled heat transfer alongside the mass transfer and did not include possible evaporation of liquid water in the model. Other assumptions included laminar flow, homogeneous porous gas diffusion layers, negligible contact resistance between the layers of the electrolyzer, normal pressure operation without the effect of capillary pressure, and conductivity as a function of temperature. The simulation model was built as a complement to an experimental setup of a electrolyzer, the results of which were used to compare and validate the results of the CFD simulation. The authors also conducted an additional simulation without the bipolar plates for comparison. COMSOL® Multiphysics was used as the solver software, but the article does not disclose the computational time and hardware used to perform the simulations. The results of the simulation were found to be adequate when compared to the experimental measurements, but the model without the bipolar plates in particular displayed discrepancies when comparing the polarization curves of the experimental model and the simulation model. The authors state that despite the ohmic losses caused by the inclusion of the bipolar plates, the results of the case were still closer to the experimental values. The non-bipolar plate -case featured higher values of current density than the measurement data, which the authors deduced to come from the lack of the aforementioned ohmic losses. The authors made additional simulations by increasing the flow channel width across 5 separate cases and discovered the effect of channel width to the current density to be miniscule. Instead, the change of channel width provided improvements to the heat transfer and reduced the total temperature of the electrolysis cell.

Another modelling study was conducted by Chen et al. (2020). The PEM-electrolyzer case was simplified to two-dimensional and included multiphase flow in the form of liquid water and gaseous hydrogen and oxygen. As the model was built as two-dimensional, the channel-wise flow direction was not included in the study: a 2-D-clipped section between the membrane and the bipolar plates on both anode and cathode side were considered instead. Alongside the simplified fluid domain, the authors also assumed laminar flow and did not include heat transfer. Therefore, only reaction kinetics of electrochemistry were modelled,

and were implemented via UDFs. ANSYS® Fluent, version unspecified, was used to solve the case. Although not directly stated in the paper, the authors calculated mass conservation equations for both phases of the model, which suggests the usage of the Eulerian multiphase model. The results of the simulation were validated against measurement data from Ojong et al. (2017) and were found to be reasonably accurate. The simulations were also compared against simulations performed Han et al., (2017), and despite the simplifications, the results were found to be close to each other. The key phenomena observed by the authors included water starvation, and the liquid water profiles, which were discovered to decrease in saturation due to the production of oxygen. The authors also discussed possible model developments, including the added effect of heat transfer, and porosity of transfer layers. The authors also considered including multidimensional analysis as a natural continuation of the simulations.

A more comprehensive CFD-simulation study was performed by Qian et al. (2022). The multidimensional fluid model featured a structure similar to Figure 4, with current collector layers included next to the anode and cathode side flow channels. The authors explained the purpose of the study the effect of operational conditions on the performance of the PEM-electrolyzer alongside the effect of the properties of the porous media. Additionally, water distribution was also investigated. The authors simplified the simulation case by not including heat transfer in the model. Turbulence was also not included, and all fluid flow was assumed to be incompressible. The authors did model the case as multiphase and utilized the mixture multiphase model in the simulations. The authors described the computational mesh to include 172 800 elements, which could be considered to be a relatively low number for an electrolyzer simulation. The paper does not discuss any refinements done to the mesh. An unspecified version of ANSYS® Fluent was used to solve the simulations with UDFs, with an Intel® i7-5000 -series central processor unit (CPU). The authors did not disclose the number of parallel processes used, or the time the software required in order to reach convergence. The results of the simulation were compared against an experiment performed “in house” according to the authors and were found to be in a good agreement. However, it should be noted that the experiment is not referenced at all in the article, nor described in detail in the article. The authors found out based on the results that higher values of current density improved water permeation through the porous membrane. Likewise, increasing the operational temperature also improved the permeation of water from the anode side to the cathode side.

Much like with alkaline water electrolysis modelling, there does not seem to be a conclusive modelling methodology found in literature when simulating PEM-electrolyzers. Multiphase models used range from Eulerian to Mixture models. In terms of software, ANSYS® Fluent has been a common tool once again alongside COMSOL® Multiphysics. It should be noted that the version differences across the software can make a significant difference when it comes to CFD simulations, which cause even more difference between different research articles when it comes to modelling methodology. It should also be noted that it is very uncommon to discuss the problems related to the solver used, which in turn leads to almost zero discussion on specific solver settings which might solve said problems during the implementation of the solver settings. Much like in literature concerning alkaline water electrolysis modelling, comparison of polarization curves is once again universally used validation method of simulations results. Many other similarities between the two electrolyzer types can be observed: studies for both range from simplified 2-D-models to more conclusive multidimensional cells. In the case of proton exchange membrane electrolyzers, the link to fuel cell research has helped in the development of recent electrolyzer models as the components are same in both applications.

2.2.3 Solid Oxide Electrolysis (SOE)

Solid oxide electrolysis differs from the previous electrolysis methods by delivering the water to the electrolyzer as steam, not liquid. This method can also be used to convert carbon dioxide into carbon monoxide, which is not doable with other electrolysis methods. Naturally, the operating temperatures of SOE are much higher than in other electrolyzers as the working fluids are all in gaseous form: the operating temperature range for a standard SOE electrolyzer is considered to be 600-900 °C (Xiang et al, 2016).

The reactions occurring during SOE can be written as:

For the anode:



And for the cathode:



Like the PEM-electrolyzer, the SOE-electrolyzer also utilizes a solid electrolyte instead of a liquid solution like in the alkaline water electrolyzer. This has been illustrated in Figure 5:

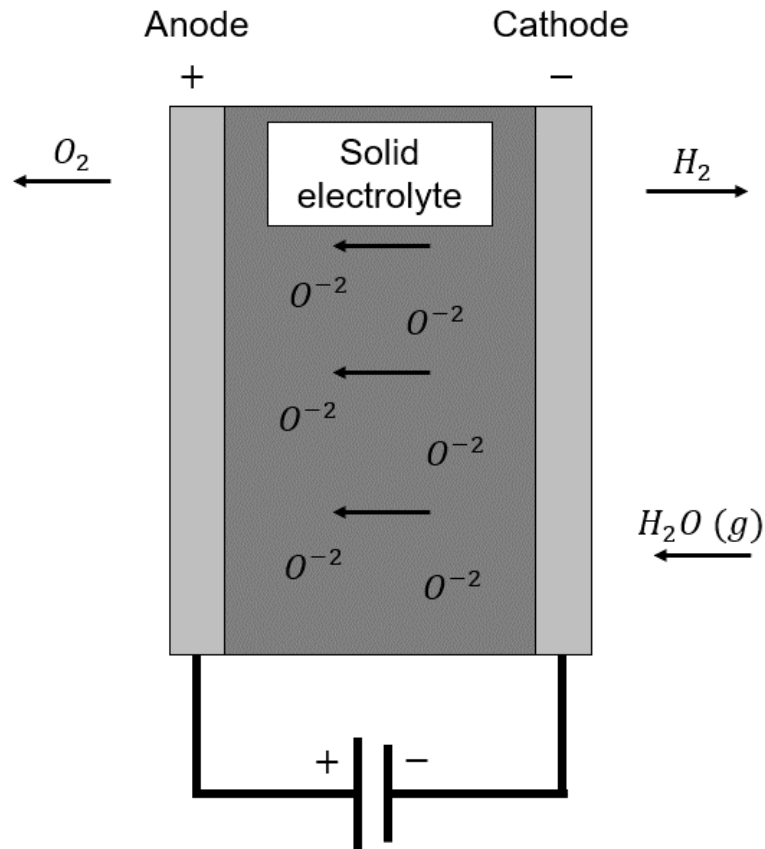


Figure 5. Basic process for a SOE-electrolyzer (Bessarabov et al., 2015, p. 3, modified from source).

As previously mentioned, the modelling research done on SOE-electrolyzers has been abundant and has followed a similar trend of research on alkaline water electrolyzers, see Figure 2. Simulation models range from analytical 0-D-models for parametric studies (Ni et al., 2007) to modern multidimensional and multiphysical CFD-models (Ho et al., 2010) (Menon et al., 2015) (Li et al., 2017) (Rizvandi & Frandsen, 2023). According to Rizvandi & Frandsen and Li et al., current research of modelling SOE-electrolyzers has been focusing more on singular electrolysis cell modelling with limitations, such as neglected heat transfer. Both authors also imply that modelling fully realized electrolyzer cell stacks and studying the operating parameters of said stacks has been receiving more research interest during recent years.

For example, a recent research article written by Rizvandi & Frandsen (2023) featured a finite element method, or FEM, simulation of a SOE-electrolyzer stack. The modelling study featured full range of physics associated with electrolysis, including mass and heat transfer, chemical reactions and charge transfer. The authors utilized COMSOL® Multiphysics as a solver, alongside MATLAB® which was used for 0-D-parameter definition and post processing. The authors studied the operational parameters of the SOE-electrolyzer stack, which included temperature and pressure. A key output parameter of the stack studied was the area-specific resistance, which was used to determine ohmic losses of the electrolyzer stack. Two geometries were implemented, one with only one-sided operation and another with double sided operation. The results were compared against experimental data provided by Jensen et al. (2016), and were discovered to reach similar values, particularly with higher values of operating pressure. The authors discovered that the double-sided geometry featured lower values of area-specific resistance, which was predictable due to the lower overpotential of the anode electrode. Likewise, the authors found out that the changes in operational pressure did not influence the distribution of current density inside the electrolyzer stacks.

3 Modelling methodology

As discovered from academic literature, the modelling methodology for PEM-electrolyzer CFD simulations varies across the studies performed on the subject. Nevertheless, this thesis attempts to perform a streamlined modelling methodology to conduct an accurate electrolysis fluid dynamics simulation using numerical methods. PEM-electrolyzer is chosen as the electrolyzer type of choice due to its close relations of fuel cells, can use essentially same methodologies to achieve results. Therefore, experience and knowledge gained from the PEM electrolyzer can directly benefit future possible fuel cell applications as well. Associated physical phenomena in the modelling methodology include multiphase flow, turbulence, heat and mass transfer, charge transfer and species transfer. A major goal for the methodology is to forgo the usage of UDFs and focus on modelling the simulation with only tools the software provides to streamline the modelling methodology as much as possible, which makes future simulations of the same topic easier to perform.

The assumptions used in the CFD simulation include the following:

1. Incompressible, laminar flow.
2. Ideal reactant gas mixtures.
3. The components and layers of the electrolyzer cell contain homogeneous materials and have constant material properties of conductance.
4. No liquid water permeation through the membrane.

Within the PEM-electrolyzer cell, liquid water with a specified mass flow rate is directed to the cell from the anode side inlet. In the anode side, the liquid water reaches the membrane of the cell where it is oxidized in the catalyst layer, where the water is split into oxygen, electrons, and hydrogen protons. The protons pass through to the cathode side of the cell, and the electrons are transported through the circuit which is simulated on the outer surfaces of the PEM-electrolysis cell. The electrons combine with the hydrogen protons at the cathode side, and form hydrogen gas which flows towards the cathode side outlet of the cell. The remaining oxygen combines with remaining electrons which did not transfer to the anode side and is transported with the remaining unreacted liquid water to the anode side outlet.

A 2-D flow schematic of the singular electrolyzer cell has been drawn in Figure 6. The figure showcases the flow direction, and the placement of the inlet and outlets.

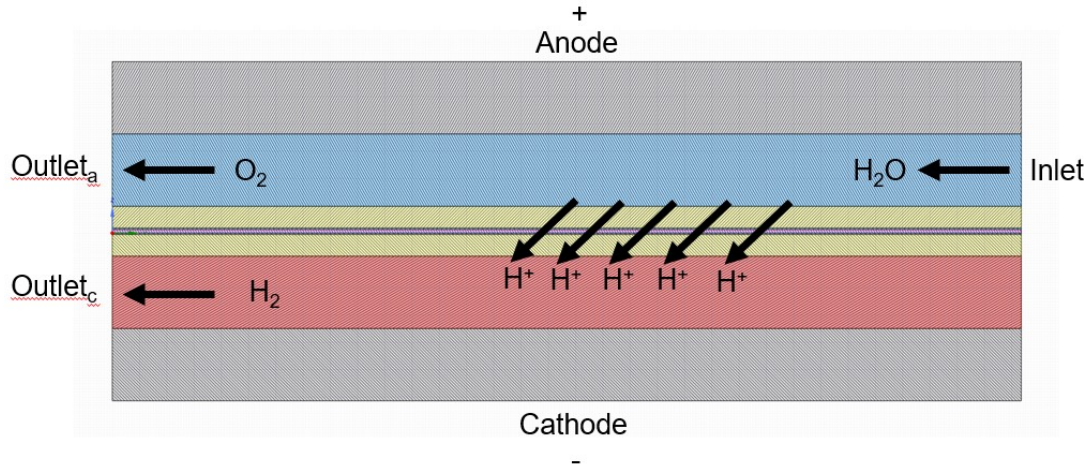


Figure 6. 2-D flow schematic of the electrolyzer cell. The schematic showcases the inlet, the outlets, and flow directions.

The modelling methodology for the PEM-electrolyzer cell CFD simulation is divided into two subchapters. The first subchapter consists of the more theoretical aspect of CFD simulations, and discloses the governing equations used to solve the fluid flow problem. This includes turbulence modelling, and the equations associated with the electrochemistry modelling. The second subchapter considers the actual building of the simulation case with the associated software. This includes the geometry model, meshing methods for said model, and finally the application of the selected solver software ANSYS® Fluent, 2023R1. Both boundary conditions and simulation settings are discussed, alongside any strategies needed to avoid common problems faced during the simulations. Essentially, the first subchapter explains what happens behind the user interface in the software and the second subchapter explains what happens on the user interface of the software.

3.1 Computational fluid dynamics

While some fluid flow problems such as simple pressure loss problems considering a piping system for example can be solved analytically with only a calculator or software such as Microsoft Excel, the complexity and simultaneity of the physics associated with electrolysis makes numerical methods necessary to provide accurate results. This is performed via

computational fluid dynamics, where numerical solver algorithms of governing equations are solved in a subdivided, or meshed, computational domain. This is also referred to as the finite volume method. According to Versteeg & Malalasekera (2007, p. 3), the algorithm can be loosely defined in three steps: in the first step the governing equations are integrated over the finite control volumes of the computational domain. In the second step the integral equations are discretised and transformed into a system of algebraic equations. Finally in the third step, the equations are solved with an iterative method.

3.1.1 Governing equations

The governing equations, also known as Navier-Stokes equations, are written for mass conservation, or continuity, momentum in all cartesian directions, and energy equation. There are multiple forms for the equations, such as integral, partial derivative etc. Here the equations are displayed in partial derivative form, based on Versteeg & Malalasekera (2007, page 24):

For the continuity equation:

$$\frac{\partial \rho}{\partial t} + \nabla \cdot (\rho \cdot \mathbf{u}) = 0 \quad (17)$$

For x-momentum:

$$\frac{\partial(\rho \cdot u)}{\partial t} + \nabla \cdot (\rho \cdot u \cdot \mathbf{u}) + \frac{\partial p}{\partial x} - \nabla(\mu \cdot \Delta u) = S_{Mx}, \quad (18)$$

For y-momentum:

$$\frac{\partial(\rho \cdot v)}{\partial t} + \nabla \cdot (\rho \cdot v \cdot \mathbf{u}) + \frac{\partial p}{\partial y} - \nabla(\mu \cdot \Delta v) = S_{My}, \quad (19)$$

For z-momentum:

$$\frac{\partial(\rho \cdot w)}{\partial t} + \nabla \cdot (\rho \cdot w \cdot \mathbf{u}) + \frac{\partial p}{\partial z} - \nabla(\mu \cdot \Delta w) = S_{Mz}, \quad (20)$$

And for the energy equation:

$$\frac{\partial(\rho \cdot i)}{\partial t} + \nabla \cdot (\rho \cdot i \cdot \mathbf{u}) + p \cdot \nabla u - \nabla(k \cdot \Delta T) = \Phi + S_i \quad (21)$$

Where ρ is density [kg/m^3], t is time [s], u , v , and w are velocities for each direction [m/s], μ is dynamic viscosity [Ns/m^2], k is heat transfer coefficient [W/mK], and Φ is the dissipation function. Additionally, S_{Mi} and S_i are the source terms for the momentum equations and energy equation respectively.

3.1.2 Turbulence

As mentioned in the assumptions of the simulations, the main simulations were simulated as laminar flow. However, comparison cases featuring turbulence were also simulated to study the effect of turbulence in the present simulation model.

Turbulence, or the irregularity of fluid flow, is modelled with a method known as Reynolds averaging, where the governing equations are dissected into two components: time-averaged, and fluctuating components. This eventually leads to a form of the governing equations called the Reynolds-averaged Navier-Stokes, or RANS equations, which now include a Reynolds stress term $-\rho\overline{u_i' u_j'}$ (Wilcox, 2006, p. 40). Multiple different variations and derivations for the RANS equations exist, which are categorized by multiple ways, including but not limited to the implementation of the Boussinesq approximation, turbulent kinetic energy, dissipation rates, length scales of turbulence etc. (Wilcox, 2006, p.26-27, 107).

To provide adequately accurate fluid flow solutions without compromising computational costs and possible instabilities when the turbulent flow is solved alongside electrochemistry and species transfer, the complete two equation k - ϵ turbulence model is used. The model was considered the most popular method to model turbulence in the 20th century, and still is widely used in many CFD applications as the turbulence model of choice (Wilcox, 2006, p. 128).

3.1.3 Electrochemistry equations

The equations presented in this subchapter are written in the same format of the solver according to ANSYS Fluent Theory Guide (2023).

The electrochemistry of a PEM-electrolyzer is built around the rates of both anodic and cathodic reactions. These reactions are driven by a variable called surface overpotential, which is defined as the difference between phase potentials of the solid phase and the electrolyte, or membrane in this case. The surface overpotentials can be depicted as:

For the anode:

$$\eta_a = \phi_{\text{sol}} - \phi_{\text{mem}} - U_a^0 \quad (22)$$

And for the cathode:

$$\eta_c = \phi_{\text{sol}} - \phi_{\text{mem}} - U_c^0 \quad (23)$$

Where U^0 is the half-cell potential for the anode and cathode respectively.

These potential terms from the surface overpotential equations can be expanded as:

$$\nabla \cdot (\sigma_{\text{sol}} \cdot \nabla \phi_{\text{sol}}) + R_{\text{sol}} \quad (24)$$

$$\nabla \cdot (\sigma_{\text{mem}} \cdot \nabla \phi_{\text{mem}}) + R_{\text{mem}} \quad (25)$$

Where σ is the electrical conductivity [$1/\Omega$], ϕ is the electric potential [V], and R is the volumetric transfer current [A/m^3]. The volumetric transfer current terms of the aforementioned equations are defined as nonzero only inside the catalyst layers, and are therefore defined as either negative or positive depending on the side of the electrolyzer: for the solid phase, $R_{\text{sol}} = -R_a (< 0)$ on the anode side and $R_{\text{sol}} = +R_c (> 0)$ on the cathode side. Likewise, for the membrane phase, $R_{\text{mem}} = +R_a (> 0)$ on the anode side and $R_{\text{mem}} = -R_c (< 0)$ on the cathode side. These volumetric transfer current terms can be defined further with the Butler-Volmer function:

For the anode:

$$R_a = (\zeta_a \cdot j_a(T)) \left(\frac{c_a}{c_a^{\text{ref}}} \right)^{\gamma_a} \left(e^{\frac{\alpha_a^a \cdot F \cdot \eta_a}{R \cdot T}} - e^{\frac{\alpha_c^a \cdot F \cdot \eta_a}{R \cdot T}} \right) \quad (26)$$

And for the cathode:

$$R_c = (\zeta_c \cdot j_c(T)) \left(\frac{c_c}{c_c^{\text{ref}}} \right)^{\gamma_c} \left(e^{\frac{\alpha_a^c \cdot F \cdot \eta_c}{R \cdot T}} + e^{\frac{\alpha_c^c \cdot F \cdot \eta_c}{R \cdot T}} \right) \quad (27)$$

Where $j(T)$ is the reference exchange current density [A/m^2], ζ is the specific active electrode surface area [$1/m$], c is the concentration of the local species [$kmol/m^3$], γ is the dimensionless concentration dependence, α is the dimensionless transfer coefficient for the anode or cathode electrode, η is the surface overpotential, see Equations (22) and (23), F is the Faraday constant, R is the universal gas constant [kJ/kgK] and T is the temperature [K].

As displayed in Equations (26) and (27), the reference exchange current densities are dependent on temperature. This connection can be written as:

For the anode:

$$j_a(T) = j_a^{\text{ref}} e^{-\frac{E_a}{RT} \left(1 - \frac{T}{T_a^{\text{ref}}}\right)} \quad (28)$$

And for the cathode:

$$j_c(T) = j_c^{\text{ref}} e^{-\frac{E_c}{RT} \left(1 - \frac{T}{T_c^{\text{ref}}}\right)} \quad (29)$$

Where E_a and E_c are the user-specified activation energy for anode and cathode [J/mol], and R is the universal gas constant [kJ/kgK].

The half-cell potentials from Equations (22) and (23) can also be expanded with a modified Nernst equation, see Equation (6) from chapter 2.1. The equation is modified to include a user-specified reaction entropy term, and is of course written for both anode and cathode:

For the anode:

$$U_a^0 = U_{a,\text{rev}}^0 - \frac{\Delta S_a}{2 \cdot F} \cdot (T - T^0) - \frac{R \cdot T}{2 \cdot F} \cdot \ln \left(\frac{p_{H_2}}{p_{op}} \right) \quad (30)$$

And for the cathode:

$$U_c^0 = U_{c,\text{rev}}^0 - \frac{\Delta S_c}{2 \cdot F} \cdot (T - T^0) - \frac{R \cdot T}{2 \cdot F} \cdot \ln \left(\frac{\frac{p_{H_2O}}{p_{op}}}{p_{\text{sat}} \sqrt{\frac{p_{O_2}}{p_{op}}}} \right) \quad (31)$$

Where U_{rev}^0 is the reversible cell potential [V] from Equation (6), ΔS_c is the user specified reaction entropy [J/K], T^0 and p^0 are temperature [K] and pressure [Pa] during standard state conditions, and p_{sat} is the saturation pressure [Pa].

As the electrolyzer produces hydrogen and oxygen in a gaseous form, the CFD model must be simulated as multiphase. In this case the mixture multiphase model is utilized, where the gas phase is considered the primary phase, and the liquid phase is considered the secondary phase. Therefore, the volume fraction for the liquid phase, water, is received from the following equation:

$$\frac{\partial}{\partial t} (v_1 \cdot \varepsilon \cdot \rho_l) + \nabla \cdot (v_1 \cdot \varepsilon \cdot \rho_l \cdot u_m) + \nabla \cdot \left(\vec{i}_m \cdot \frac{n_d}{F} \cdot M_{H_2O(l)} \right) = S_1 \quad (32)$$

Where v_1 is the volume fraction for the liquid phase, ε is the porosity, ρ_l is the density of the liquid phase [kg/m^3], u_m is the velocity for the whole mixture [m/s], n_d is the osmotic drag coefficient, \vec{i}_m is the ionic current density [A/m^3], F is the Faraday constant, $M_{H_2O(l)}$ is the molar mass of water in liquid state, and S_1 is the source term for the liquid phase from the electrochemistry reactions.

The source term S_1 can be expanded for the liquid phase as:

$$S_1 = -\frac{M_{H_2O(l)}}{2 \cdot F} \cdot R_a \quad (33)$$

Where R_a is the anodic volumetric transfer current from Equation (26). Likewise, the source terms for the gaseous phases can in turn be written based on the molar masses as:

$$S_{H_2} = \frac{M_{H_2}}{2 \cdot F} \cdot R_c \quad (34)$$

$$S_O = \frac{M_{O_2}}{4 \cdot F} \cdot R_a \quad (35)$$

The aforementioned volumetric source terms are only calculated at the catalyst layers of the electrolyzer model and are set as zero in the other layers. Additional source terms must be included in the energy equation, since it is not possible to convert all the electrical energy into chemical energy in an electrolyzer: the excess electrical energy will dissipate as heat energy. The thermal source terms differ depending on the section of the electrolyzer, and can be written as:

For the current collectors and the gas diffusion layers:

$$S_{CC} = \frac{i_{sol}^2}{\sigma_{sol}} \quad (36)$$

For the anode side catalyst layer:

$$S_{CL,a} = \frac{i_{sol}^2}{\sigma_{sol}} + \frac{i_{mem}^2}{\sigma_{mem}} + R_a \left(-\eta_a - \frac{T \cdot \Delta S_a}{n \cdot F} \right) \quad (37)$$

And for the cathode side catalyst layer:

$$S_{CL,c} = \frac{i_{sol}^2}{\sigma_{sol}} + \frac{i_{mem}^2}{\sigma_{mem}} + R_c \left(-\eta_c - \frac{T \cdot \Delta S_c}{n \cdot F} \right) \quad (38)$$

And finally for the membrane:

$$S_{mem} = \frac{i_{mem}^2}{\sigma_{mem}} \quad (39)$$

Where i_{sol} is the current density of the solid phase [A/m^3], i_{mem} is the current density of the membrane phase [A/m^3], and η_a and η_c are the surface overpotentials [V] from Equations (22) and (23) for the anode and cathode respectively.

As the electrolyzer cell features liquid water transport in porous regions, which is driven by pressure gradients, the effect of capillary pressure must also be present in the modelling. The capillary pressure of the electrolyzer cell can be obtained from the Leverett function, depicted as:

$$p_c = \sigma \cdot |\cos\theta_c| \cdot \sqrt{\frac{\varepsilon}{K}} \cdot J(x) \quad (40)$$

Where σ is the surface tension [N/m], θ_c is the contact angle [deg], ε is the porosity, and K is the absolute permeability of the porous medium [m^2]. Additionally, the $J(x)$ term can be expanded as:

$$J(x) = a \cdot x - b \cdot x^2 + c \cdot x^3 \quad (41)$$

Where a , b , and c are user specified coefficients for the Leverett function, and x is length of the medium.

With the capillary pressure defined, the liquid water transport in porous medium can now be defined as:

$$\frac{\partial}{\partial t} (\varepsilon_i \cdot \rho_l \cdot s) = \nabla \cdot \left(\frac{\rho_l \cdot K \cdot K_r}{\mu_l} \cdot \nabla (p_c + p) \right) + S_{gl} - S_{ld} \quad (42)$$

Where s is the liquid saturation, K_r is the relative permeability of the porous medium [m²], p_c is the capillary pressure from Equation (40) [Pa], and S_{gl} and S_{ld} are the source terms for mass transfer between phases: S_{gl} represents the mass transfer between gas and liquid phases, and S_{ld} represents the mass transfer between liquid and dissolved phases. The gas-liquid mass transfer source term S_{gl} can be written as:

$$S_{gl} = \begin{cases} \gamma_{er} \cdot \varepsilon \cdot s \cdot D_{gl} \cdot \frac{M_{H_2O}}{RT} \cdot p \cdot \ln\left(\frac{p - p_{sat}}{p - p_{wv}}\right), & p_{wv} \leq p_{sat} \\ \gamma_{cr} \cdot \varepsilon \cdot (1 - s) \cdot D_{gl} \cdot \frac{M_{H_2O}}{RT} \cdot p \cdot \ln\left(\frac{p - p_{sat}}{p - p_{wv}}\right), & p_{wv} > p_{sat} \end{cases} \quad (43)$$

Where γ_{er} is the evaporation rate coefficient, γ_{cr} is the condensation rate coefficient, and p_{wv} is the pressure of water as vapor [Pa]. The diffusion coefficient for the gas to liquid phase mass transfer D_{gl} is a function of both temperature and pressure, and can be expanded as:

$$D_{gl} = \begin{cases} 0,365 \cdot 10^{-4} \cdot \left(\frac{T}{343}\right)^{2,334} \cdot \left(\frac{10^5}{p}\right), & \text{cathode} \\ 1,79 \cdot 10^{-4} \cdot \left(\frac{T}{343}\right)^{2,334} \cdot \left(\frac{10^5}{p}\right), & \text{anode} \end{cases} \quad (44)$$

The source term for mass transfer between liquid and dissolved phases can be in turn written as:

$$S_{ld} = s^\theta \cdot \gamma_{ld} \cdot M_{H_2O} \cdot \frac{\rho_{mem}}{EW} \cdot (\lambda_{eq} - \lambda) \quad (45)$$

Where γ_{ld} is the user defined liquid mass exchange rate constant, ρ_{mem} is the density of the membrane [kg/m³], EW is the equivalent weight of the membrane [kg], and λ is the dissolved water content. The equivalent dissolved water content λ_{eq} can in turn be expanded to

$$\lambda_{eq} = 0,3 + 6a(1 - \tanh(a - 0,5)) + 0,69(\lambda_{a=1} - 3,52)a^{0,5} \left(1 + \tanh\left(\frac{a-0,89}{0,23}\right)\right) + s(\lambda_{s=1} - \lambda_{a=1}) \quad (46)$$

Where a is the water activity, defined as the ratio of pressure of water vapor and saturation pressure. The water contents $\lambda_{s=1}$ and $\lambda_{a=1}$ are both user-defined.

3.2 Simulation workflow

The CFD simulation performed in the thesis can be divided into six steps, which have been depicted in Figure 7:

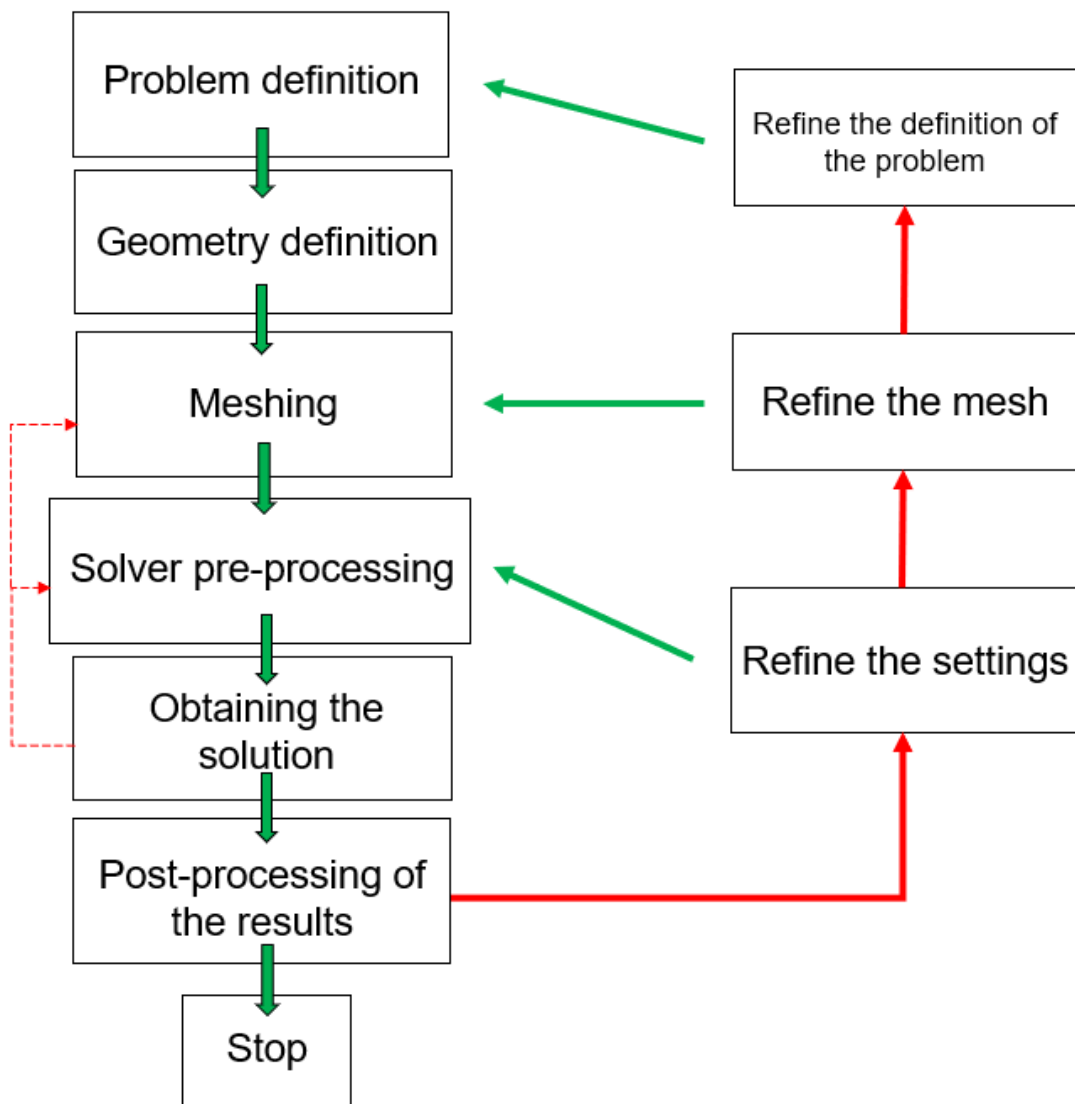


Figure 7. Iterative process of the CFD simulation.

As one can observe from Figure 7, the process of conducting CFD simulations can and almost always is iterative in nature. The steps displayed in the figure can be defined as:

1. Problem definition. In the first step, the goals, scope, and scale of the simulated application is defined and researched. Simplifications and assumptions to be used in the simulation will also be defined in the first step, alongside the boundary conditions and other input parameters used in the numerical simulation. In certain applications, the to-be-simulated fluid flow problem definition may include analytical calculations beforehand.
2. Geometry definition. In the second step, the geometry of the defined problem from step 1 is built using CAD, or computer assisted design- software. The geometry is built as the fluid domain, which at minimum must feature an inlet, which dictates the surface where the fluid flow is directed to the control volume, an outlet, which dictates the surface where the flow exits the control volume, and walls.
3. Meshing. In the third step, the geometry of the control volume of the fluid domain is subdivided into smaller elements, or cells, where the governing equations will be solved. The quality of the mesh can affect the obtained solution with major effect, which makes the third step one of the more often iterated steps in the simulation workflow.
4. Solver pre-processing. In the fourth step, the mesh is brought into the solver software, where the boundary conditions can be implemented. Alongside the boundary conditions, additional solver settings must be implemented and set up properly. This includes and is not limited to discretization methods of the mesh, the choice of pressure-velocity-coupling scheme, relaxation factors, the number of iterations the solver takes to run the case and setting up monitor parameters and functions to monitor the solver during the simulation. After the appropriate settings have been implemented, the fluid flow case can then be initialized, the method which can also have effect on the running of the case.
5. Obtaining the solution. In the fifth step, the initialized case from the previous step is simulated the number of iterations specified. While often the most straightforward step of the simulations, the simulation step of the workflow is usually the one step where most problems can present themselves. These problems can be related to convergence issues or stability issues for example. Therefore, sometimes the iterative process of the workflow can manifest itself even before any results have been

obtained, which can be observed from Figure 7. Certain applications of CFD simulations also prefer to implement certain features and physics in a step-by-step basis, such as implementing the energy equation only after running the fluid flow problem without heat transfer for a couple hundred iterations. The solver simulation is considered complete when the governing equations reach convergence. This is usually defined with the residuals of the equations, which ideally decrease towards zero as much as possible during the simulation. Likewise, the aforementioned monitors can be used to determine convergence.

6. Post-processing of the results. In the final step, the results obtained from the previous step are processed and exported from the solver software. This includes any data deemed useful at the very first step of the simulation workflow, such as figures of contour plots, streamlines, vectors, or values of user-defined expressions such as surface integrals of specific parameters. As presented in Figure 7, after analyzing the results, if the results are not deemed satisfactory or accurate enough, one must return to a previous step of the CFD workflow and either refine the solver settings or boundary conditions, or the mesh, or in the worst case even the definition of the problem.

As demonstrated in the introduction of the thesis, the goal of the simulations is to model a singular straight channel PEM-electrolyzer cell. The geometry model was developed using ANSYS® SpaceClaim, which was then exported to ANSYS® Workbench for meshing. The mesh was then exported to ANSYS® Fluent, which was used for both pre- and post-processing. Additional analytical calculations were performed with Excel. All commercial ANSYS® Software used were version 2023 R1.

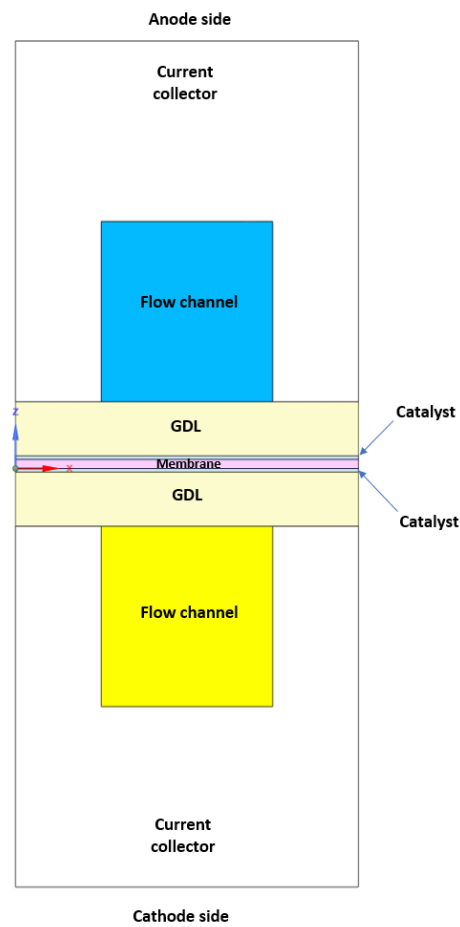
3.2.1 Geometry description

The geometry for the single electrolysis cell was built according to the dimensions from the research article written by Toghyani et al., (2018). The dimensions of the geometry domain have been depicted in Table 1:

Table 1. Dimensions of the PEM-electrolyzer cell.

Location	Value	Unit
Cell length	50	[mm]
Cell height	4,69	[mm]
Cell width	2	[mm]
Membrane thickness	50	[μm]
Catalyst thickness	20	[μm]
Gas Diffusion Layer thickness	300	[μm]
Current Collector thickness	1000	[μm]
Flow channel width	1	[mm]
Flow channel height	1	[mm]

Figure of the different layers of the electrolyzer cell from a Z-X-clip plane can be seen from Figure 8. An isometric view of the entire cell can in turn be seen from Figure 9:

**Figure 8.** Clip plane of the electrolyzer cell, with annotations for each layer.

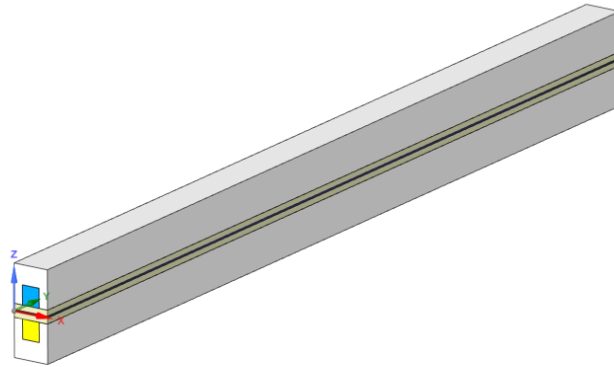


Figure 9. Isometric view of the electrolyzer cell.

The surrounding current collectors are modelled as solid bodies, and every other component is considered to be the fluid volume of the computational domain.

In order for the solver to recognize the components of the electrolyzer cell, different named selections of the layers of the cell were created. This also included electrical tabs for both anode and cathode side, which were placed at the top and bottom surfaces of the current collectors: top surface for the anode side and bottom surface for the cathode side. These tab surfaces would indicate to the solver where the electrical current is conducted into the computational domain. Alongside tabs, bodies for current collectors, gas diffusion layers, catalysts, flow channels and the membrane were named. No walls or internal boundaries were necessary to name at this stage, as the solver would automatically designate said boundaries after applying the electrochemistry model.

After the base case PEM-electrolyzer cell geometry was complete, it was exported to ANSYS® Workbench for meshing.

3.2.2 Mesh

As mentioned during the overview on computational fluid dynamics and simulation workflow description, the purpose of meshing is to subdivide the control volume developed

as a 3-D CAD model into smaller separate regions, or cells, where the governing equations and electrochemistry equations will be solved. More specifically, the solution is obtained at nodes, which are connecting points between the divided cells of the computational domain. Therefore, the quality of the mesh can have major effects on the accuracy of the results of the CFD simulation: the more cells, and therefore nodes, the mesh has, the more solutions can be obtained for the domain. Naturally this also leads to increased computational cost and time spent on the simulation, as the governing equations will be solved for more nodes. (Versteeg & Malalasekera, 2007, pages 3-6)

ANSYS® Workbench was used as the software for creating the grid. The software allows the user to generate grids one part at a time, which allows more stable and controlled mesh generation. The mesh controls used for the grid generation have been depicted in Table 2:

Table 2. Mesh controls for the base case grid.

	Value	Unit
Default Element size	0,1	[mm]
Catalyst y-axis divisions	6	-
Membrane y-axis divisions	10	-

The number of y-axis divisions from Table 2 refer to how many sublayers the catalyst layers and the membrane will be divided into in y-direction, see Figure 8 for reference. Additionally, mesh inflation layers were implemented to the gas diffusion layers, directed towards the catalysts with growth rate of 1,2. Likewise, the edge sizing of the membrane was enhanced with a hard bias towards the catalysts. With the aforementioned settings, a structured mesh consisting of 800 000 elements was generated. The generated mesh can be seen from Figure 10. Enhanced images of the gas diffusion layers, catalyst layers and membrane can in turn be seen from Figure 11. The latter figure showcases the inflation and the hard bias implemented in the gas diffusion layers and membrane.

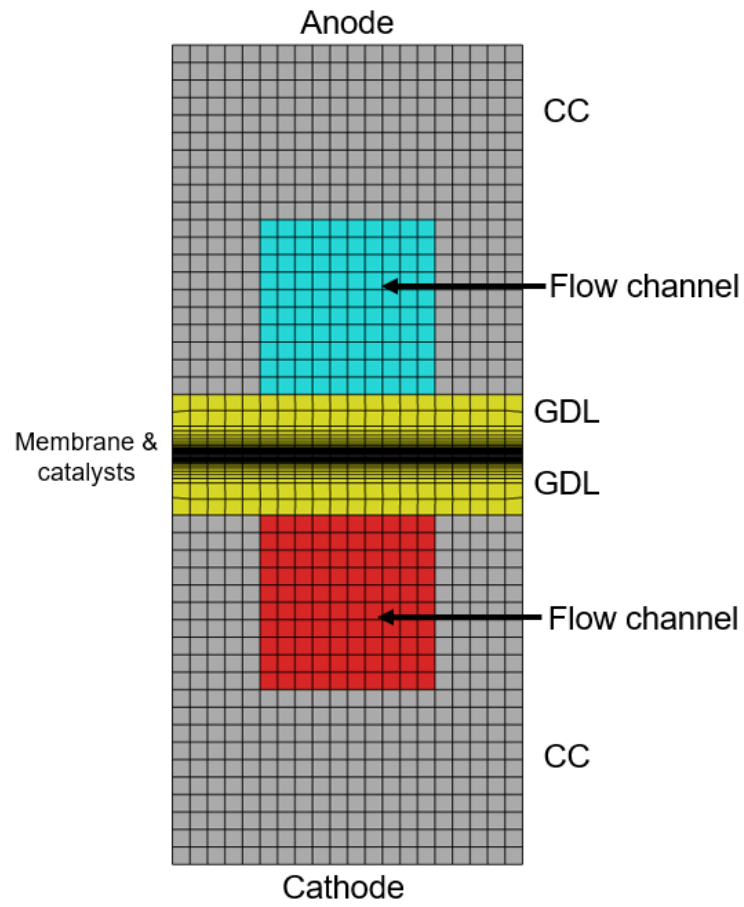


Figure 10. Z-X-clip of the mesh with annotations.

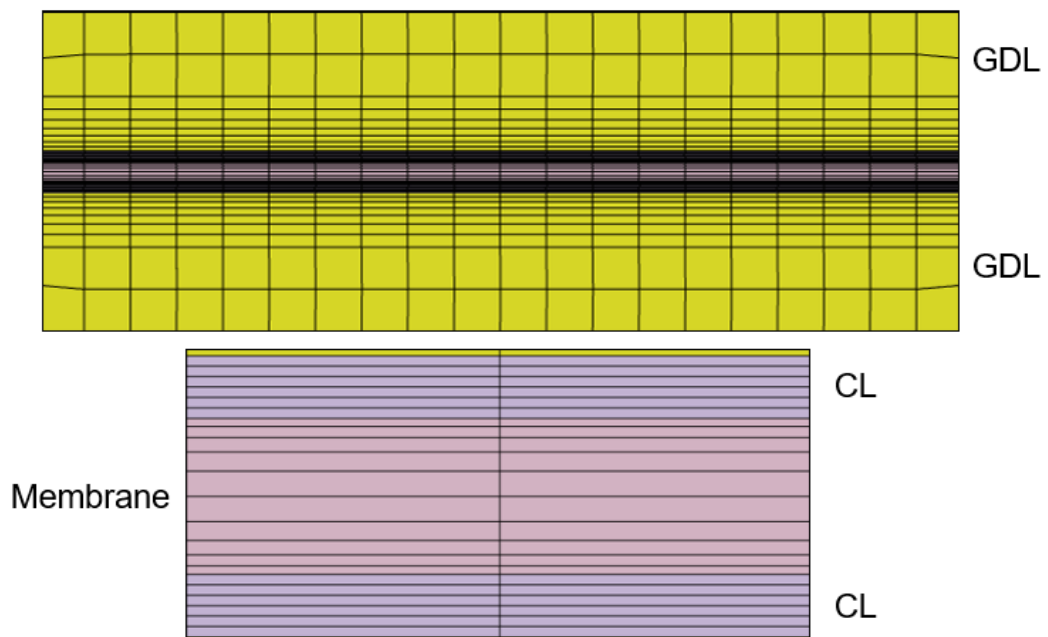


Figure 11. Enhanced images of gas diffusion layers, catalysts, and the membrane.

An important factor of any numerical CFD study is to ensure that the results obtained are as grid independent as possible. This is commonly performed by building multiple progressively finer meshes of the same geometry and obtaining the solution for all of them. Then the output values of a single parameter are compared to determine when the number of elements in the mesh no longer affects the solution.

In the present work, the volume-integrals of the volumetric transfer current at catalyst layers were chosen as the parameter for the grid independence study. Five meshes were generated with progressively higher total element counts, and were solved with the same boundary conditions, and with the same total voltage of 1,702 V. The transfer currents obtained from the simulations can be seen from Figure 12:

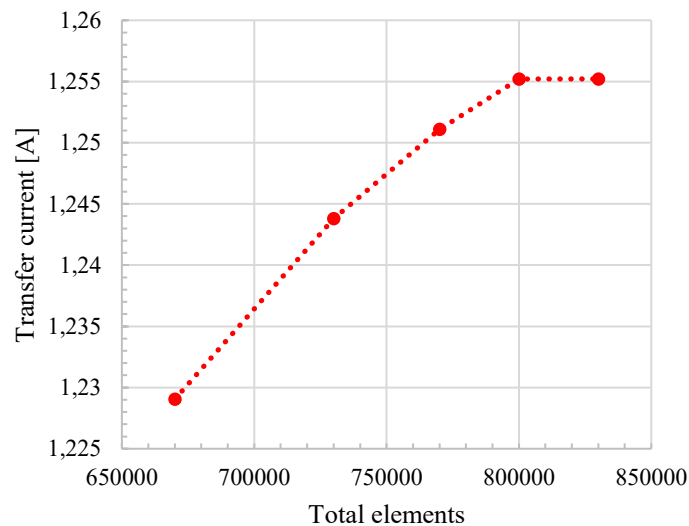


Figure 12. Grid independence study for the electrolyzer simulation.

One can observe from Figure 12 that element counts past 800 000 elements start to display diminishing changes in the transfer current. The grid independence test procedure was naturally done before the other results were obtained from any simulation, which lead to the final decision to use the 800 000-element count mesh as the grid for all simulations from there on.

3.2.3 Solver settings and boundary conditions

Commercial software ANSYS® Fluent 2023R1 was used for the preprocessing, solving, and postprocessing of the simulations. The solver was set up as pressure-based and steady-state. After setting up the general settings of the solver, the electrochemistry model was enabled.

The module enables two potential equations, see Equations (22) and (23) from chapter 3.1.3, which allows the simulation of charge transfer in the cell. Additionally, the model automatically enables both the energy equation for material definition and heat transfer purposes, and species transport equations for the species transfer. The electrochemistry model can be ran based on either total voltage of the cell, or total current of the cell. In this thesis, all simulations were performed as voltage based. Therefore, total voltage of the electrolyzer cell was specified as user input instead of defining the total current of the cell as input. From the general settings of the model, electrochemistry sources were enabled, which enables all the electrochemistry equations alongside the potential equations. Additionally, Butler-Volmer rate equations were also enabled, which correspond to Equations (26) and (27). Osmotic drag and capillary pressure were also enabled for increased accuracy. The capillary pressure refers to Equations (40-46).

The electrochemistry model requires some constant user defined parameters to function. These values remain constant across all simulations, and have been catalogued in Table 3:

Table 3. Model parameters for the electrochemistry model.

Parameter	Unit	Anode	Cathode	Global
J^{ref}	[A/m ²]	1,36E-09	1500	-
E	[J/mol]	62836	24359	-
C^{ref}	[kmol/m ³]	1	1	-
Con. Exponent	-	0	0	-
Exchange coefficient a	-	2	1	-
Exchange coefficient c	-	2	1	-
Open voltage	[V]	-	-	1,1999

Where J^{ref} is the reference exchange current density j_a^{ref} and j_c^{ref} , and E is the activation energy E_a and E_c from Equations (28) and (29), C^{ref} is the reference concentration c_a^{ref} and c_c^{ref} from Equations (26) and (27), “Con.Exponent” is the dimensionless concentration dependence γ_a and γ_c from Equations (26) and (27), and the exchange coefficient a and c are

the charge transfer coefficients α_a^a and α_a^c for both sides from Equations (26) and (27). The open voltage corresponds to the constant open-circuit voltage for anode-side half-cell potential U_a^0 from Equation (30), which is set as constant value when the electrochemistry model is not ran with half-cell voltage setting enabled. The activation energies seen in Table 3 were chosen based on the estimations made by Chandesris et al. (2015) in their study of membrane degradation in PEM-electrolyzers.

After setting up the model parameters for the cell, the components defined and named during the creation of the geometry were identified and assigned appropriately for each zone for both anode- and cathode sides, including the tab surfaces. The properties for the aforementioned zones have been depicted in Table 4:

Table 4. Properties for the porous zones in the electrolyzer cell.

Component	Parameter	Unit	Anode	Cathode	Mem
Gas diffusion layer	Porosity	-	0,5	0,5	-
	Absolute permeability	[m ²]	1,00E-12	1,00E-12	-
	Contact angle	[deg]	70	60	-
	Leverett coeff. a	-	1,417	1,417	-
	Leverett coeff. b	-	2,12	2,12	-
	Leverett coeff. c	-	1,263	1,263	-
Catalyst layer	Porosity	-	0,2	0,2	-
	Absolute permeability	[m ²]	4,90E-12	2,00E-12	-
	Surface volume ratio	[1/m]	20000	20000	-
	Contact angle	[deg]	80	60	-
	Leverett coeff. a	-	1,417	1,417	-
	Leverett coeff. b	-	2,12	2,12	-
	Leverett coeff. c	-	1,263	1,263	-
Membrane	Porosity	-	-	-	0,5
	Absolute permeability	[m ²]	-	-	4,70E-09

The values for porosity and permeability were chosen based on the study performed by Toghyani et al., (2018). The rest of the values are default values of the solver, except for the contact angles, which were chosen to be at 10 degrees and 20 degrees difference in the gas diffusion layers and catalyst layers respectively for increased stability for when the solver iterates the fluid flow in the porous regions and especially in the contact areas between porous and non-porous regions. The Leverett coefficients a-c refer to the capillary pressure Equation (41) and are also default values of the solver.

After choosing the correct named bodies from the geometry, including the tab surfaces for both anode and cathode side, applying the electrochemistry model automatically updated cell zones and walls for the electrolyzer. Alongside, energy equation was automatically enabled, as was the species transport equation and the mixture multiphase model. The mixture model formulated the volume fraction parameters as implicit and considered the phases as dispersed. The primary phase was automatically set to be the gas phase, named “pem-mixture” in the software, and liquid water as the secondary phase. The “pem-mixture” consists of hydrogen, oxygen, nitrogen, and water as vapor. The material properties of the phases were left as their default values.

The material properties of the homogeneous components and layers can be seen from Table 5:

Table 5. Material properties for the components of the electrolyzer cell.

Component	Parameter	Unit	Value
Current collector	Thermal conductivity	[W/mK]	100
	Electrical conductivity	[S/m]	20000
	Electrolyte conductivity	[S/m]	1,00E-16
Gas Diffusion Layer	Thermal conductivity	[W/mK]	10
	Electrical conductivity	[S/m]	20000
	Electrolyte conductivity	[S/m]	1,00E-16
Catalyst layer	Thermal conductivity	[W/mK]	10
	Electrical conductivity	[S/m]	5000
	Electrolyte conductivity	[S/m]	4,5
Membrane	Thermal conductivity	[W/mK]	2
	Electrical conductivity	[S/m]	1,00E-16
	Electrolyte conductivity	[S/m]	11

The boundary conditions were implemented to match the measurement conditions provided by Debe et al. (2012). Flow rate of 300 ml/min, or 0,005 kg/s of liquid water was set to the mass flow inlet, alongside the operating temperature of 360,65 K. It should be noted that the measurements featured a varied temperature between 353,15 K and 368,15 K. Therefore, an average temperature is used in the simulations. Total voltage of the electrolyzer cell varied from 1,498 V to 1,765 V. Operational pressure likewise varied in the measurements from 1 atm to 100 psig, or from 1,01 bar to 6,89 bar. Average pressure value of 3,954 bar was used

for the simulations as the boundary condition for the pressure outlets. The boundary conditions of the electrolyzer cell have been summarized in Table 6:

Table 6. Boundary conditions for the electrolyzer simulation.

Boundary	Parameter	Unit	Value
Anode inlet	q_m	[kg/s]	0,005
	$T_{in, a}$	[K]	360,65
Anode outlet	$p_{out, a}$	[bar]	3,954
Cathode outlet	$p_{out, c}$	[bar]	3,954
Global	Total voltage	[V]	1,498...1,765

Based on the boundary conditions from Table 6, mainly the anode inlet mass flow rate, and dimensions of the geometry from Table 1, we can estimate the inlet Reynolds number for the purposes of studying the effect of implementing a turbulence model to the simulations. Reynolds number can be obtained from the equation (White, 1998, p. 24):

$$Re = \frac{\rho \cdot v \cdot L_h}{\mu}$$

Where v is the velocity of the fluid flow [m/s], L_h is the characteristic length [m], and μ is the dynamic viscosity of the fluid [Ns/m²], which for liquid water in the operational temperature of 360,65 K within the electrolyzer cell is 0,000324 Ns/m² (Incropera et al., 2011, page 933). The characteristic length of a rectangular for a rectangular flow channel, such as the inlet surface of the simulated geometry, is expressed as the hydraulic diameter of the channel d_h :

$$L_h = d_h = 4 \cdot \frac{A}{U_p} \quad (47)$$

Where U_p is the wetted perimeter of the duct [m]. The Reynolds number can now be estimated as:

$$Re = \frac{\rho \cdot v \cdot 4 \cdot \frac{A}{U_p}}{\mu} \quad (48)$$

With assumed density of 1000 kg/m³, The Reynolds number from Equation (48) would give a value of 20 576.

With the estimated Reynolds' numbers, the pressure loss of the electrolyzer cell can be solved analytically for verification purposes. This can be done with the Darcy-Weisbach - equation and is written as (White, 1998, p. 367, derived from source):

$$\Delta p = \frac{f_D \cdot \rho \cdot v^2 \cdot L}{2 \cdot d_h}, \quad (49)$$

Where f_D is a dimensionless friction factor, L is the length of the flow channel [m], and d_h is the hydraulic diameter of the duct from Equation (47). The dimensionless friction factor is expressed with the Colebrook equation as a function of Reynolds' number and the relative surface roughness of the duct wall (White, 1998, p. 348) and has a value of 0,0297 with an estimated surface roughness of 0,002 mm, which is common for well-maintained sheet metal (White, 1998, p. 349). The friction factor can also be determined empirically from Moody-charts. With the same estimated density of 1000 kg/m³, flow velocity of 5 m/s, channel length of 100 mm, see Table 1, and hydraulic diameter from Equation (47) of 0,0013 m, we can predict the pressure loss of the electrolyzer cell to be 12 051 Pa, or ~ 0,12 bar.

The pressure-velocity coupling of the simulations was performed with the "SIMPLE" scheme, and all spatial discretization schemes were selected to be performed with first order upwind schemes. Converge criteria was set for the residuals of the governing equations as 1E-6. Alongside, the volumetric transfer currents at the catalyst layers and volume-integrated velocities at the gas diffusion layers, catalyst layers and membrane were set as monitor parameters to determine if convergence had been reached. After either reaching convergence or near-convergence, the heat transfer of the electrolyzer was enabled by enabling Joule-heating and reaction heat from the electrochemistry-model, after which the solver was allowed to continue to iterate the solution until convergence was reached.

Another method for pressure-velocity coupling includes the "Coupled" scheme, which allows the user to manipulate the pseudo-transient global time step of the steady state flow. This is done with a variable called time scale factor, which adjusts the automatically calculated size of pseudo time step formulated from the minimum fluid time scales of equations representing the different physics associated with the fluid flow, which include convection, buoyancy, gravitation, etc. The time scale factor scales the global time step size, to a smaller or higher value, which often increases convergence. In the present work, the "Coupled" scheme was run for comparisons between the pressure-velocity coupling methods in electrolyzer simulations. After initializing the solution, time scale factor was set to 0,1 for

the first 100-200 iterations, after which the time scale factor was reduced to 0,001. After another 100-200 iterations, the time scale factor was reduced again to its final value of 0,0001 until the solution was converged. Like with the “SIMPLE” scheme, joule heating and reaction heat were enabled at this stage.

The simulations were performed with an Intel® Xeon® W-2275 3,30 GHz CPU, of which 12 of the 14 available logical parallel processes were used. The solver was run with double precision.

4 Simulation results

The simulation results were extracted directly from Fluent, either as direct images or as data exported to and plotted in Excel.

Polarization curve for the electrolyzer cell has been depicted in Figure 13:

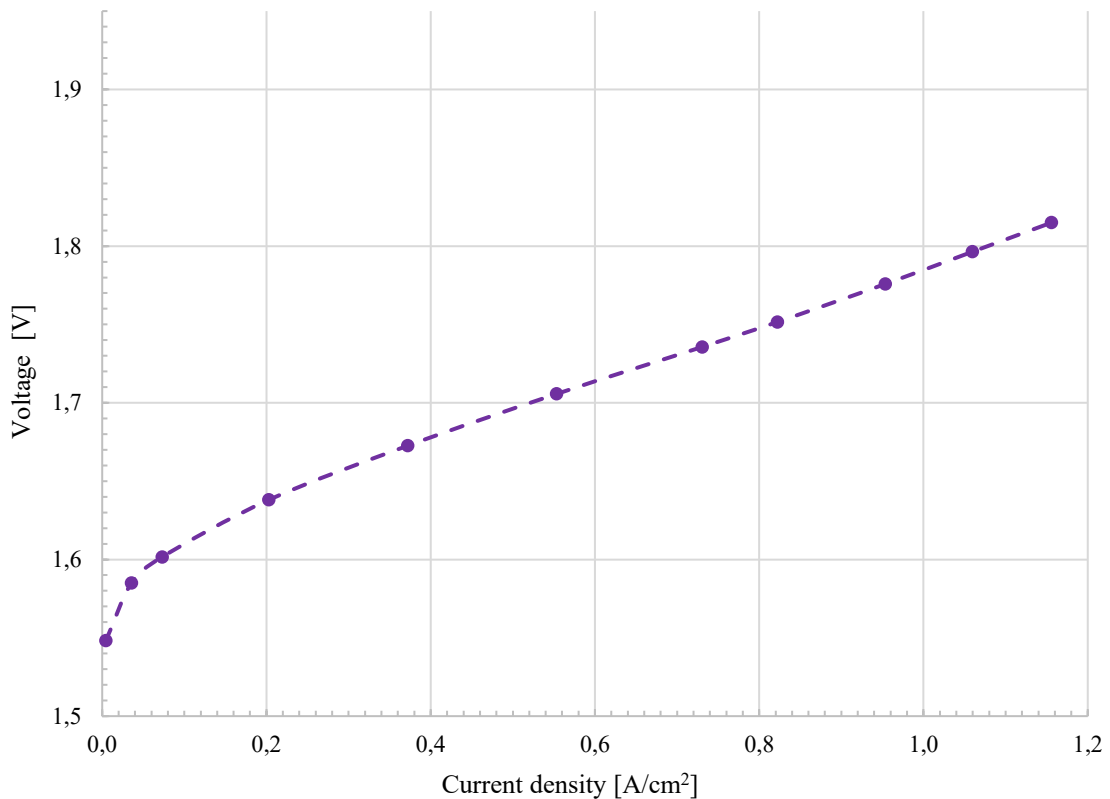


Figure 13. Polarization curve for the simulated electrolyzer cell.

Contours of current density for three selected voltages across a ZX clip-plane of the electrolyzer cell can be seen from Figures 15 and 16. The voltages were chosen to represent the low section, middle section, and high section of the polarization curve. The clip plane was taken from between the middle of the electrolyzer and the outlets, at $y = 0,0125$ m. Certain results have been plotted alongside on a ZY-clip from the middle of the cell, at $x = 0,001$ m. The clip plane locations have been visualized in Figure 14:

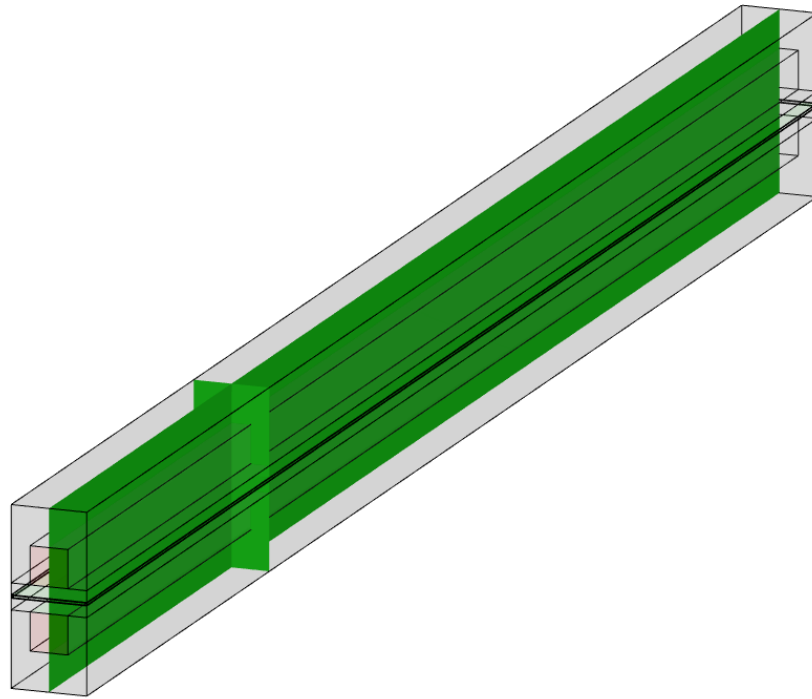


Figure 14. Locations for the clip planes inside the electrolyzer cell.

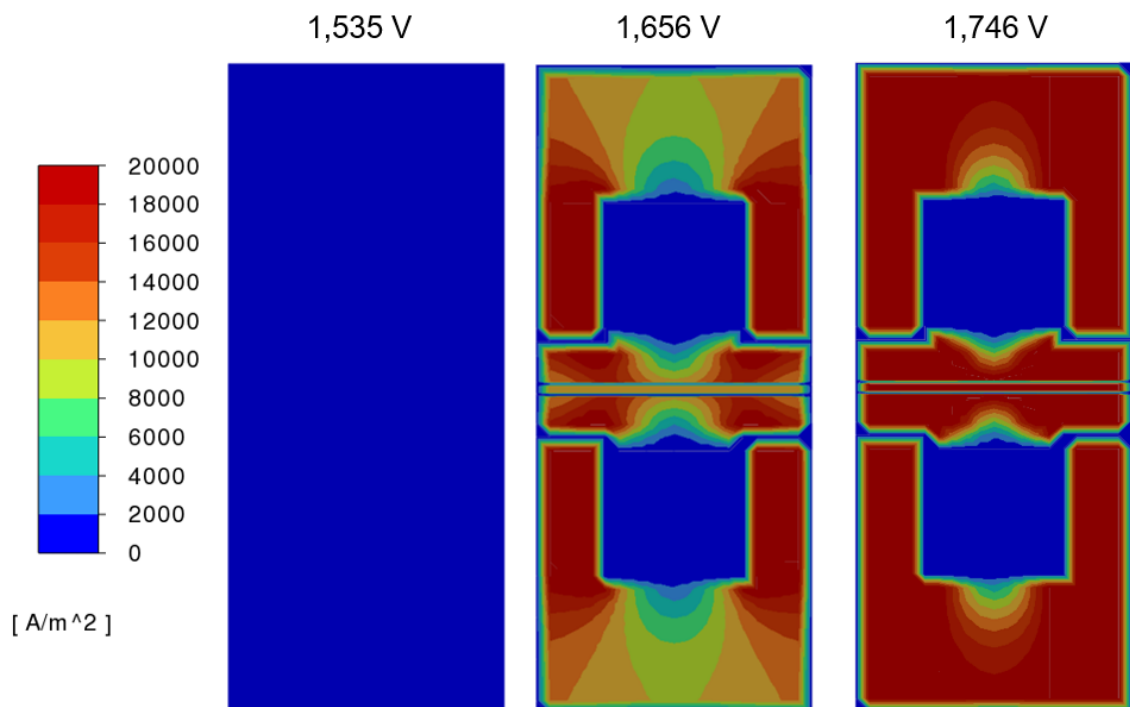


Figure 15. Contours of current density magnitude on a ZX-clip plane for three voltages.

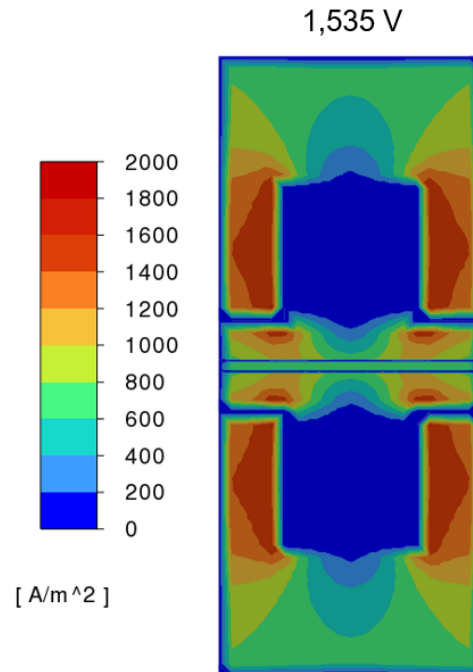


Figure 16. Downscaled version of the current density magnitude contour for the 1,535 V case.

The total output of the hydrogen mixture phase flowing out of the cathode side for both pressure-velocity coupling schemes have been catalogues in Table 7:

Table 7. Mass flow rates for the hydrogen mixture phase in the cathode side outlet for three voltages, from both schemes.

SIMPLE (laminar)		Coupled (turbulent)	
U [V]	$q_{m,c,out}$ [kg/s]	U [V]	$q_{m,c,out}$ [kg/s]
1,535	7,44E-10	1,535	7,44E-10
1,656	1,16E-08	1,656	1,16E-08
1,746	2,23E-08	1,746	2,21E-08

4.1 Results with the “SIMPLE” scheme

Contours of the hydrogen mixture phase volume fraction solved with the SIMPLE pressure-velocity coupling has been depicted in Figures 17 and 18. The total output of the hydrogen mixture phase flowing out of the cathode side have been catalogued in Table 7:

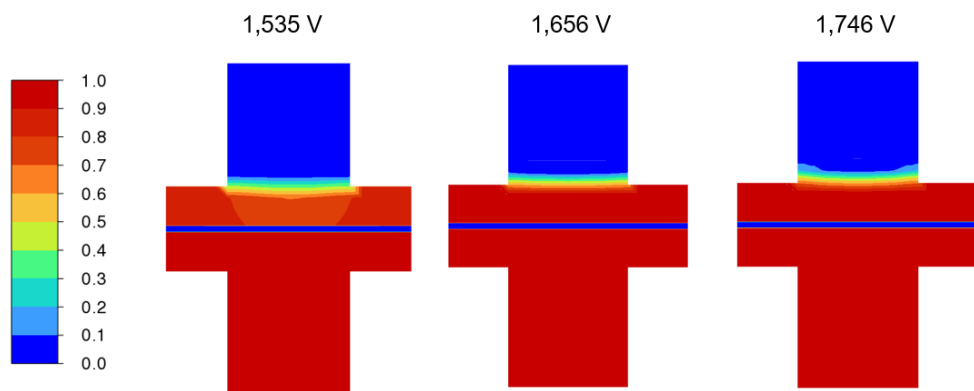


Figure 17. Contours of volume fraction of hydrogen mixture phase on a ZX-clip for three voltages solved with the SIMPLE pressure-velocity coupling.

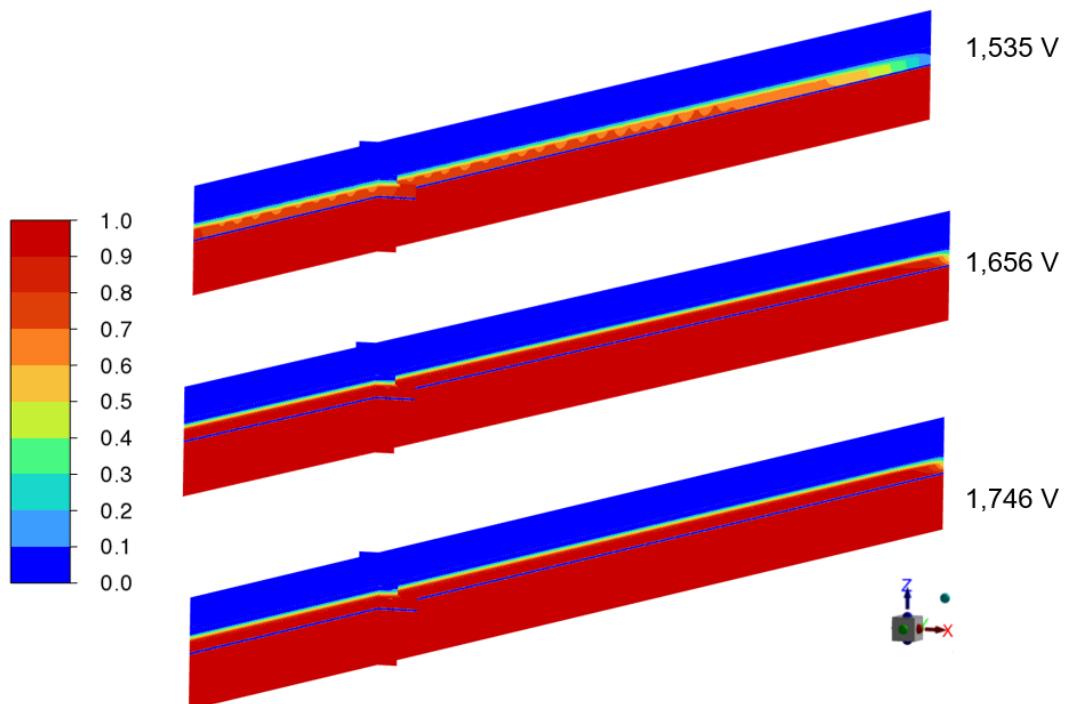


Figure 18. Contours of volume fraction of hydrogen mixture phase on a ZY-clip for three voltages solved with the SIMPLE pressure-velocity coupling.

Contours of velocity magnitude have been plotted in Figures 19 and 20. Additionally, velocity contours have been plotted at a lower scale at the same clip plane only on the GDLs, CLs and the membrane in Figure 21. The maximum velocities reached in the cells were calculated from the anode side of the cell, and had the range of values from 5,0 to 7,05 m/s. The contours use lower scaling to demonstrate how the fluid flow develops on the cathode side as the voltage of the cell is increased.

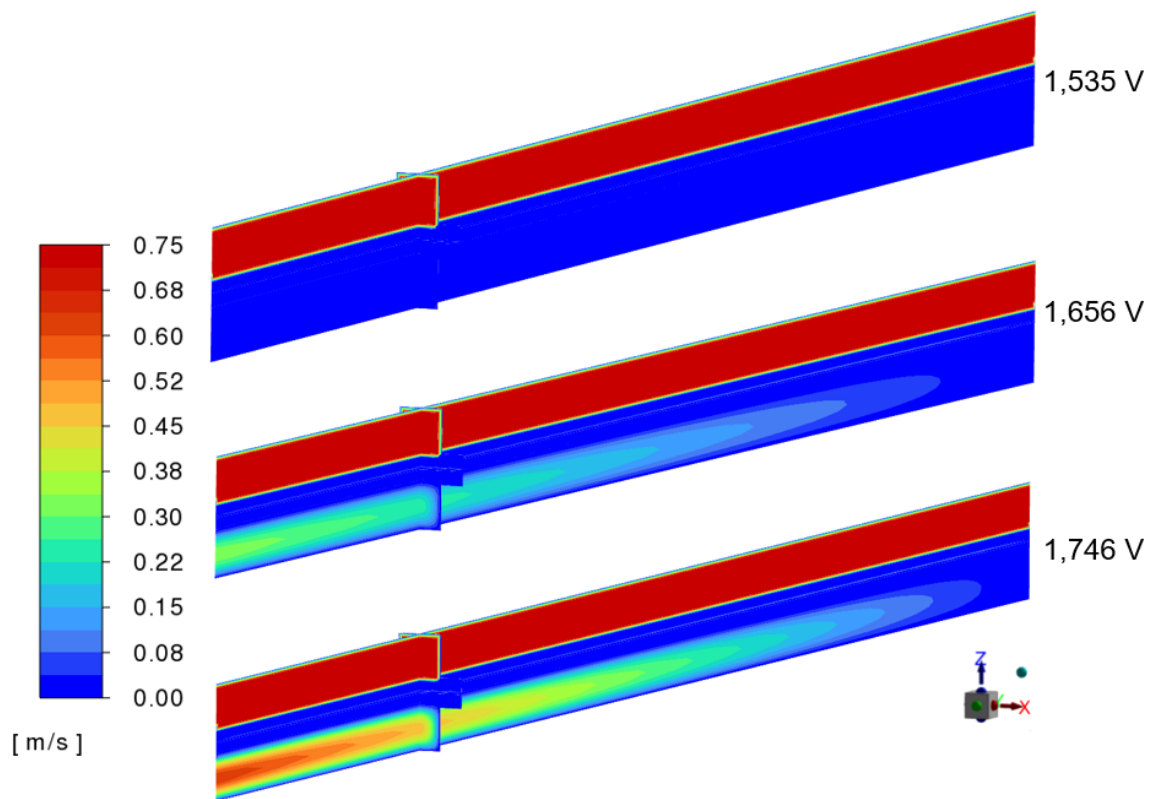


Figure 19. Contours of velocity magnitude plotted on ZX and ZY-clip planes for three voltages.

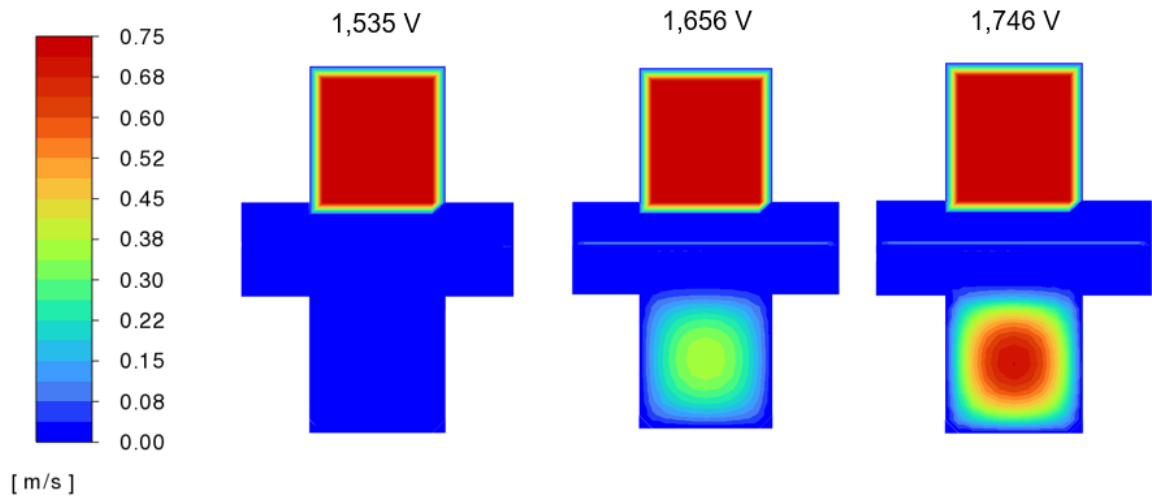


Figure 20. Contours of velocity magnitude plotted on ZX clip planes for three voltages.

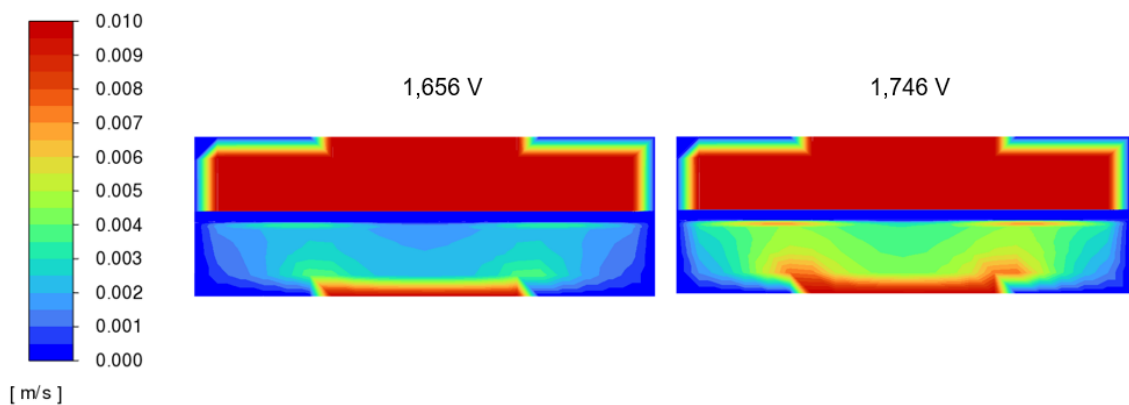


Figure 21. Contours of velocity magnitude plotted on two higher voltages on the ZX-clip plane, only on GDLs, CLs, and the membrane.

Contours of static pressure have been plotted in Figure 22. The total pressure loss of the electrolyzer cell remained constant across all voltages, which was 0,14 bar for the laminar flow with SIMPLE pressure-velocity coupling.

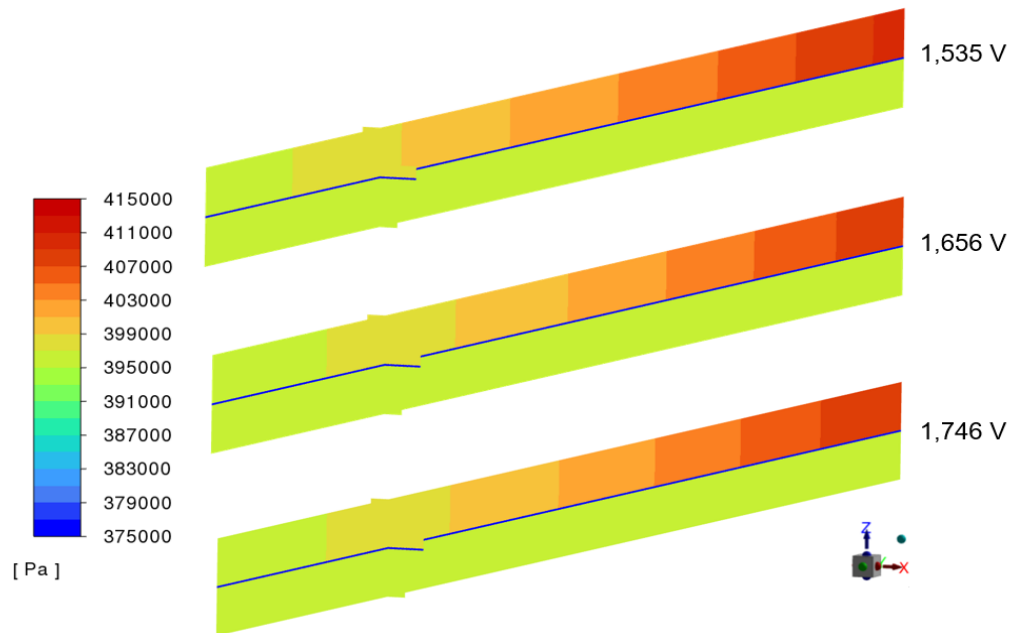


Figure 22. Contours of static pressure plotted on ZX and ZY-clip planes for three voltages solved with the “SIMPLE” scheme.

4.2 Results with the “Coupled” scheme

Contours of the hydrogen mixture phase volume fraction solved with the “Coupled” pressure-velocity coupling has been depicted in Figures 23 and 24:

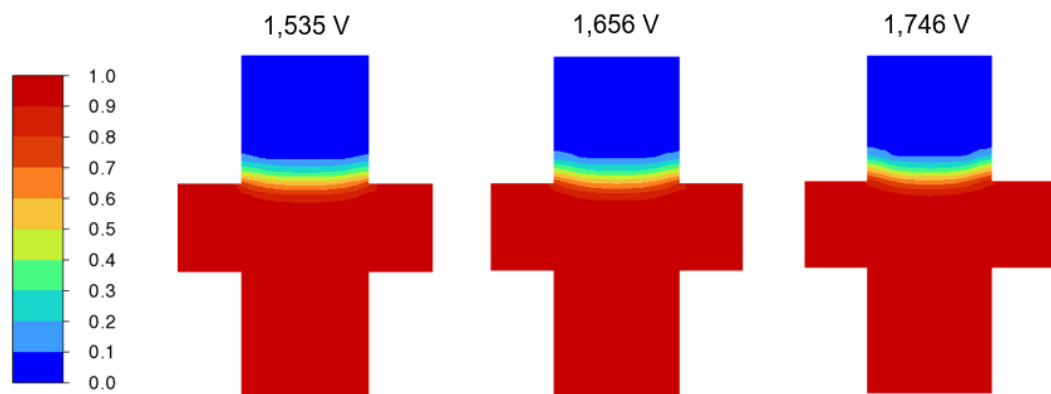


Figure 23. Contours of volume fraction of the hydrogen gas mixture phase solved with the “Coupled” scheme, plotted on the ZX clip plane.

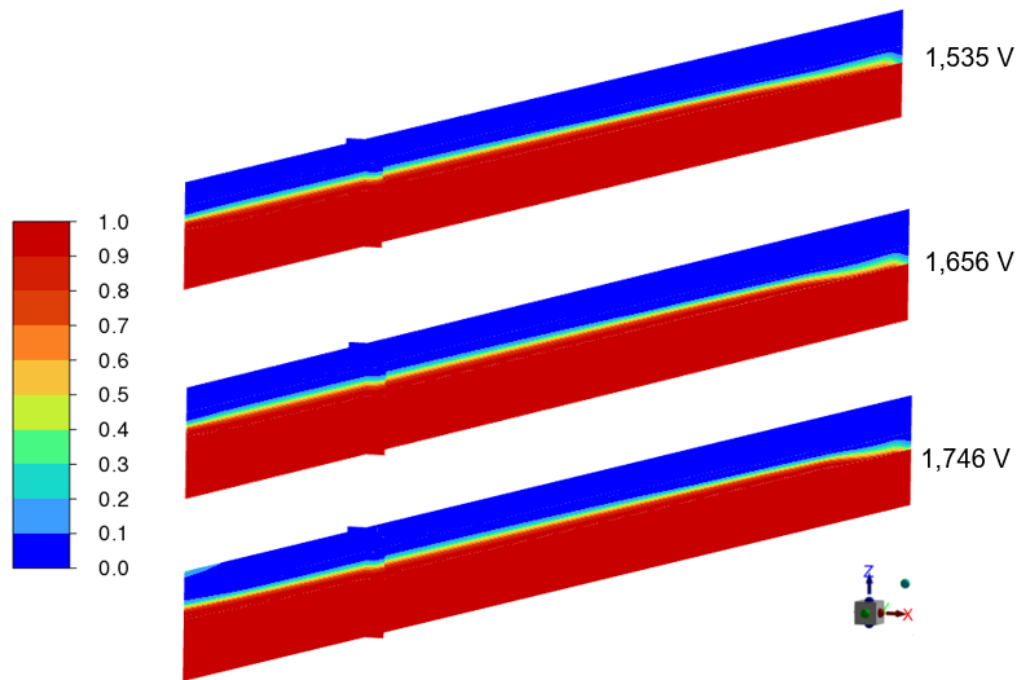


Figure 24. Contours of volume fraction of the hydrogen gas mixture phase solved with the "Coupled" scheme on both ZX and ZY clip planes.

The laminar velocity contours did not change between the SIMPLE and Coupled coupling schemes. Instead, the turbulent flow comparison case velocities solved with the Coupled scheme have been plotted in Figure 25, for all the clip surfaces, Figure 26 for ZX-clip only, and Figure 27 for lower scale for the GDLs, CLs and membrane:

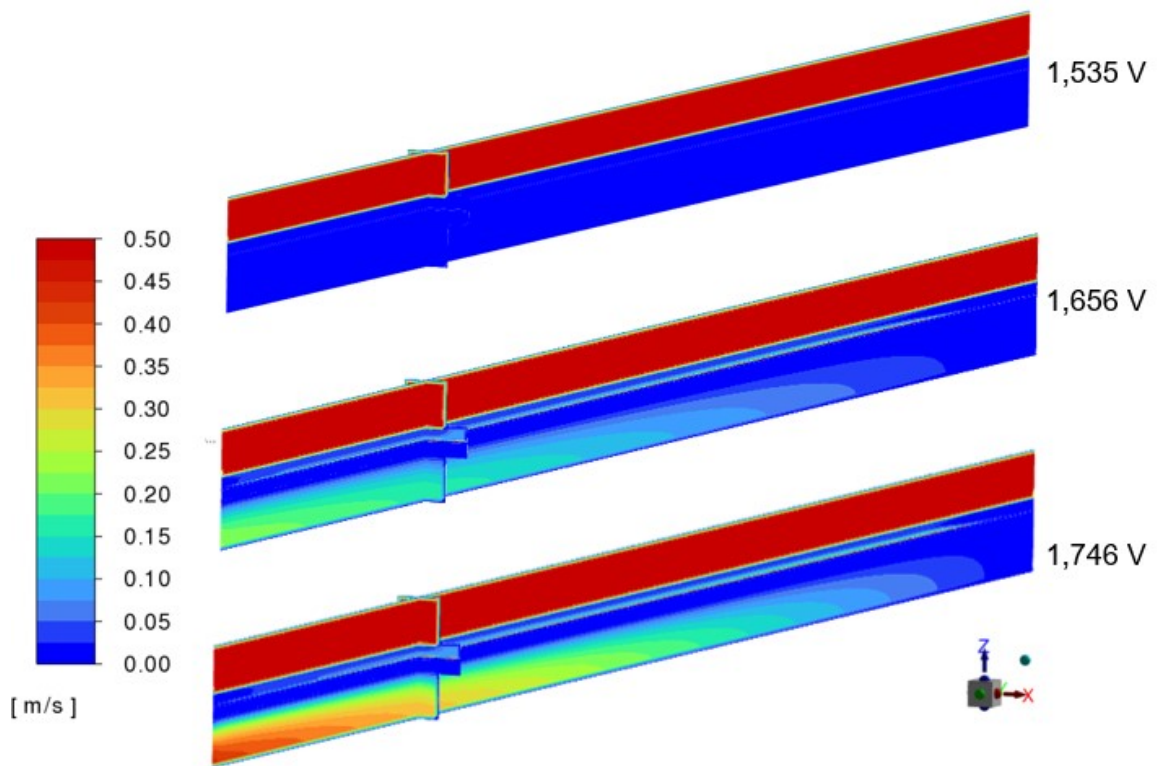


Figure 25. Contours of velocity magnitude solved with the "Coupled" scheme with turbulence.

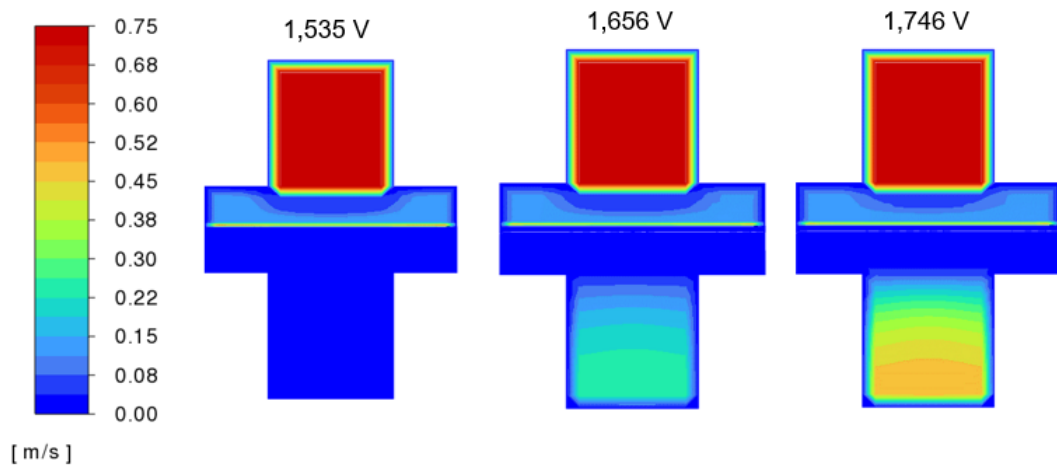


Figure 26. Contours of velocity magnitude solved with the "Coupled" scheme with turbulence, plotted in the ZX-clip plane.

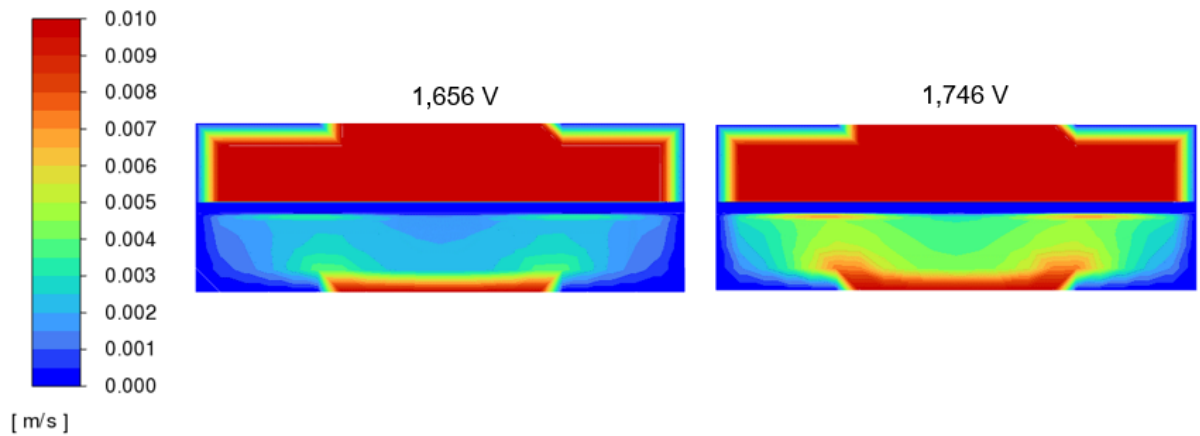


Figure 27. Contours of velocity magnitude plotted on two higher voltages on the ZX-clip plane, only on GDLs, CLs, and the membrane, with turbulence.

The inclusion of turbulence also affected the pressure levels of the electrolyzer, which has been plotted in Figure 28. For comparison, the laminar fluid flow case solved with the Coupled scheme can in turn be seen from Figure 29:

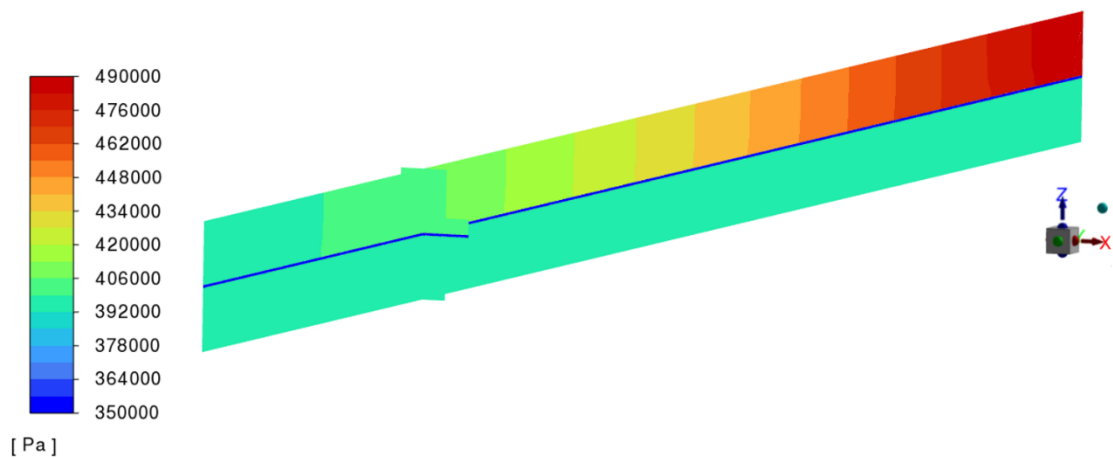


Figure 28. Pressure contours of the electrolyzer solved with the "Coupled" scheme with turbulence. The pressure contours remained identical across the varied three voltages.

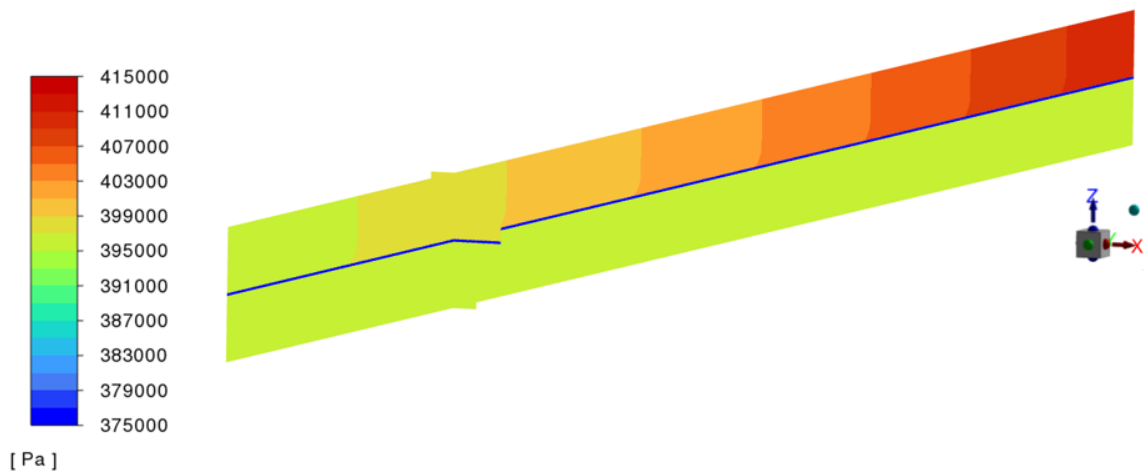


Figure 29. Pressure contours of the electrolyzer solved with the "Coupled" scheme without turbulence. Like with the turbulence simulations, the contours remained identical across the three voltages.

As mentioned in the literature review, a major goal for many PEM electrolyzer simulations is to find optimal operating points, conditions, and properties for the cell in order to maximize the performance-to-cost ratio. This is especially relevant for PEM-electrolyzer due to the major costs of the catalysts. To demonstrate a possible optimization, additional simulations were conducted to study the effect of membrane thickness on the polarization curve of the cell. The simulations were performed with the same mesh controls and element count; only the membrane thickness was altered in the CAD-software. Membrane thicknesses of 30 μm , 50 μm , 100 μm and 200 μm were used for the comparisons. The polarization curves plotted based on the result data of the additional simulations can be seen from Figure 30:

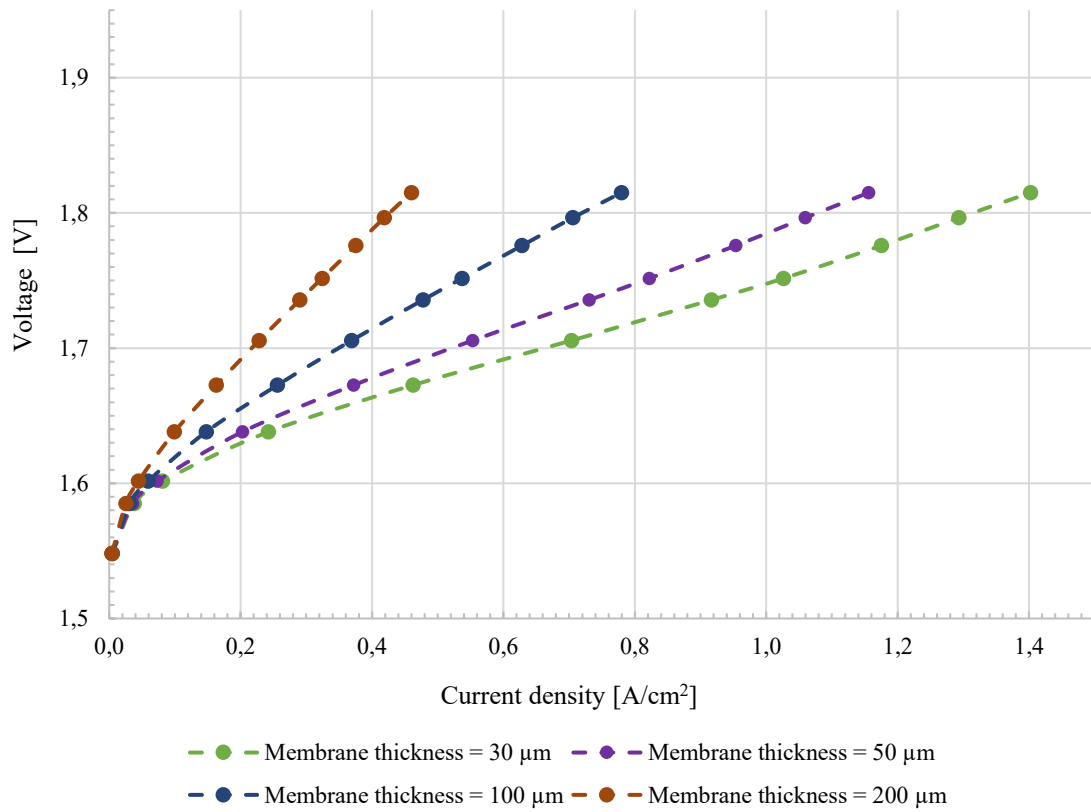


Figure 30. Simulation results for different values of membrane thickness and their effect on the polarization curve of the cell.

5 Discussion of results

As discovered from academic literature, the most common method for simulation validation and measurement for the accuracy of CFD simulations when modelling electrolyzers is the comparison of polarization curves. A comparison between the polarization figures from both simulation results and measured data can be seen from Figure 31:

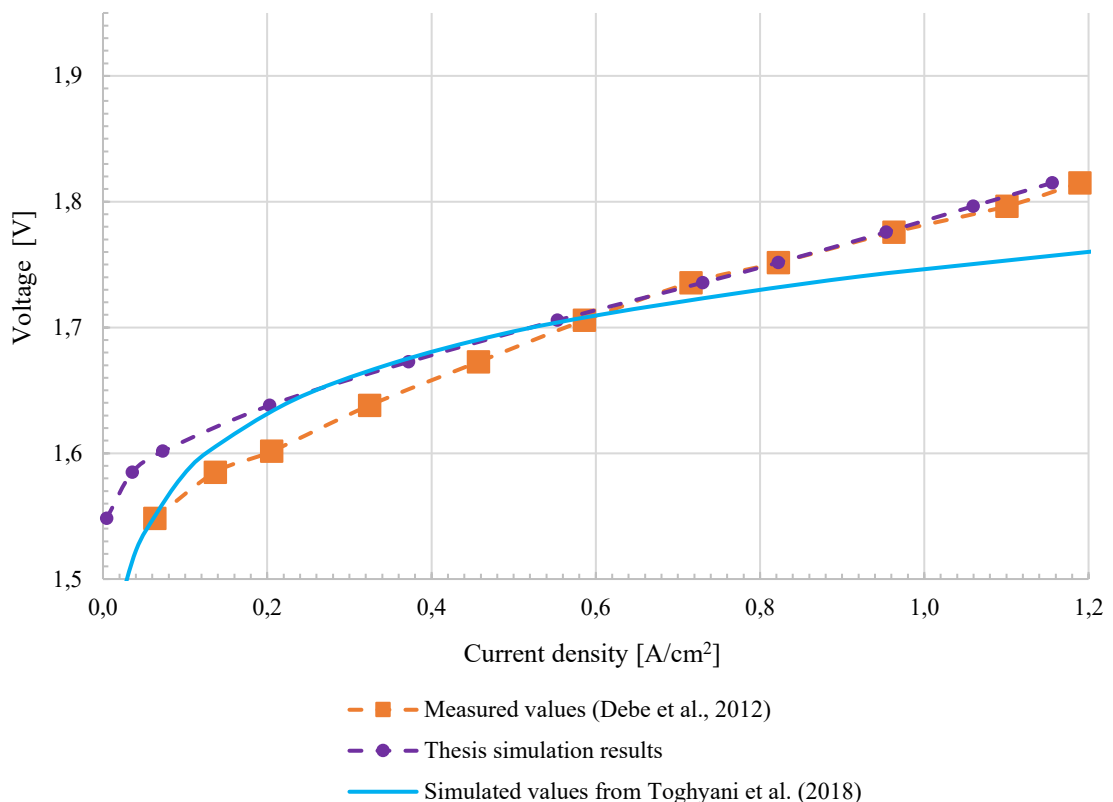


Figure 31. Simulation results alongside measurements from Debe et al. (2012) and CFD-simulations performed by Toghyani et al. (2018) on the same polarization curve.

Based on the comparison of polarization figures, it can be concluded that the model provides adequately accurate results performance-wise. The only major discrepancies occur at lower voltages, a phenomenon which was discovered to be relatively common across multiple studies performed on the subject. However, the CFD simulations provided satisfactory results as the voltage was increased. Similar agreements were discovered also in the CFD study performed by Toghyani et al. (2018), where the simulated electrolyzer cell seemed to yield lower values of current density at lower voltages when compared to the same measured

data. However, the study also had more discrepancies at higher voltages as well, which is not present at the simulation results performed in this thesis. The differences between the present simulations and simulations performed by Toghyani et al. most likely come from the implementation of the electrochemistry equations. The study utilized UDFs with self-written equations, whereas the present model only used the built-in tools for the software. Another major difference between the two CFD simulations was the fact that the study ran the simulations only with one phase, which can also affect the overpotential equations. By contrast, in the present simulation the volumetric transfer currents are directly connected to the mixture multiphase model, see Equation (32).

Key phenomenon validated from the results is the increase in cell performance as the voltage of the cell is increased. This can be especially noticed at the lowest values of voltage, where the current through the cell is miniscule as displayed in Figures 15 and 16. Likewise, the cell approaches near-zero values of current density at lower voltages. This is also showcased in the hydrogen mixture volume fraction contours, where one can observe how the hydrogen production is increased as the voltage increases. This can be seen from the 1,535 V case ZY-clip, where the hydrogen mixture develops much further in the cell than in the cases with higher voltage. The observations made are complemented by the total mass flow rate for the hydrogen phase in cathode side in Table 7, where the increase in voltage increased the total mass flow rate of the outlet boundary. The table also shows the severe drop in produced hydrogen when running the electrolyzer with the lowest values of voltage, dropping from $1,16\text{E-}8$ kg/s to $7,44\text{E-}10$ kg/s when the voltage was reduced from 1,656 V to 1,535 V.

When comparing the volume fractions of the hydrogen mixture phase, the contours seem almost identical between the SIMPLE laminar and Coupled turbulent simulations. The volume fractions in the turbulent simulations seem to reach further into the anode side, even with the lower cell voltages. By comparison, similar phenomenon is displayed only in the 1,746 V case in the laminar cases. Another interesting phenomenon is displayed at the low voltage of 1,535 V in the laminar case, where the hydrogen is produced fully further into the flow channel. This is mostly due to the low voltage of the cell, which corresponds to low transfer currents, which in turn corresponds to the multiphase volume fraction Equation (32). Interestingly, the same phenomenon is not present at the turbulent cases, with the same voltage. This is also reflected in Table 8, where total hydrogen mixture phase mass flow rates are depicted. It could be deduced that the inclusion of turbulence had almost zero effect

on the amount of hydrogen produced, since the volume fraction for the hydrogen mixture phase was identical at the cathode side for both laminar and turbulent simulations. Turbulence would however have an effect on the flow pattern of the produced hydrogen instead, which was displayed in the velocity contours.

The application of turbulence can be an important factor in the case of an electrolyzer simulation. In the case of the present model, the Reynolds number at the anode-side inlet was calculated to be 20 576, which would be classified as a fully turbulent flow in a rectangular flow channel. For comparison, the outlet velocities for the anode side were measured in the software and were 5,33 m/s for the anode side, and 0,36 m/s for the cathode side in the simulations with turbulence included. This would translate to Reynolds numbers of 21 954 at the anode-side outlet, and 1495 at the cathode outlet respectively. Therefore, fluid flow in the cathode side can be considered to be fully laminar, and flow in the anode side can be considered to be fully turbulent, which validates the use of the turbulence model. It should however be noted that the inclusion of turbulence had no effect on the performance of the cell, despite its effect on the pressure losses: The added effect of turbulence increased the pressure loss of the cell from 0,16 bar to 0,95 bar with the “Coupled” pressure-velocity coupling, which can be observed when comparing the pressure contours from Figures 28 and 29.

The pressure losses of the cell in the SIMPLE scheme simulations were constant 0,14 bar, which has a difference of 0,02 bar to the laminar Coupled scheme simulation. The inlet pressures for the simulations were 4,10 bar for the laminar SIMPLE scheme simulations, 4,12 bar for the laminar Coupled scheme simulations, and 4,90 bar from the turbulent Coupled scheme simulations. When comparing to the pressure estimations made in chapter 3.2.3 with the Darcy-Weisbach Equation (49), the pressure loss based on friction of the flow channel was estimated to be $\sim 0,12$ bar. This is in good agreement with the simulations without turbulence modelling enabled but has more discrepancy with the simulations where turbulence model was enabled, having a difference of 0,83 bar. Differences could be caused most likely by the estimation of surface roughness, which assumes that the gas diffusion layer-side of the flow channel has equal surface roughness to the current collector sides, which is most likely not the case. Additionally, the discrepancy between the estimated pressure loss and the loss obtained from the turbulent simulation can be from the mesh used in the simulation. In the present mesh, there are no additional boundary layers in the flow

channel segment of the geometry, which is due to the desire to keep the mesh as structured as possible due to the porous layers of the electrolyzer cell. Likewise, the mesh is quite coarse at the flow channels, which can affect the accuracy for the obtained shear stresses caused by friction, which affect the pressure losses of the channel.

One possible factor which should be considered in the model is the pressure at the anode and cathode outlets. In an actual electrolyzer, these values would not necessarily be same. Typically, pressure on the cathode side can be lower than in the anode side, which can affect the performance of the electrolyzer. In this simulation, an average pressure was used based on the listings made in the article by Debe et al. (2012). The pressure levels within the electrolyzer cell are difficult to verify as the measurements performed by Debe et al., were mostly on performance of the cell with different membrane materials and testing facilities. This also makes hydrodynamic results of the simulation difficult to validate, an issue which was discovered to be a relevant problem in the academic literature as well.

The velocity contours showcase the differences in the flow patterns when the turbulence model was implemented. The turbulent simulations showcased higher velocity gradients in the anode side CL and GDL. However, it should be noted that when inspecting the middle section of the cell, no major differences were found between the laminar and turbulent velocity patterns, at least not at such as low scale.

The results obtained from the membrane thickness study demonstrate how much direct influence membrane thickness has on electrolyzer performance. As observed from Figure 30, there is room for membrane thickness adjustment in the present model, as the 30 μm membrane produced higher values of current density in the electrolyzer cell. By comparison, the thicker membranes of 100 μm and 200 μm display increased ohmic losses and ohmic resistance of the cell, as the charge and hydrogen protons must pass through a thicker membrane to reach the cathode side of the cell. Similar conclusions were made by Toghyani et al. (2018) in their CFD study.

The solver performance during the simulation was also monitored in the “Coupled” scheme simulations, by extracting parallel performance data from Fluent after convergence was reached. The data received include the total number of iterations, average wall clock time per iteration, and total wall clock time of the whole simulation. Data was taken from the same three voltage cases as before, and has been depicted in Table 8:

Table 8. Parallel performance data extracted from the solver for the Coupled scheme simulations.

Voltage [V]	Total iterations -	Average time per iteration [s]	Solver total runtime [s]
1,535	1492	1,77	2290
1,656	1220	1,75	2136
1,746	990	1,80	1781

Based on the information received from the parallel performance data, one can deduce that the lower voltage-cases take longer to solve when compared to higher and more middle voltage values. The 1,535 V case took approximately 38 minutes to converge, and the 1,656 V case took approximately 36 minutes to reach convergence. The difference between the 1,656 V and 1,746 V was considerably smaller by comparison. The differences between voltages become even more apparent when considering a larger geometry with a more complicated flow pattern.

It should be noted that the SIMPLE pressure-velocity coupling simulations were much more unstable but took less time to converge when compared to the Coupled scheme, especially when solving the higher voltages. Typically, the solver required at least 200-400 iterations to “find” the solution for the species transfer equations. After the species transfer equations converged, the solver quickly also managed to obtain the solution for the continuity equation and reach convergence.

5.1 Best practices for electrolyzer simulations

Most of the problems encountered during the simulations presented themselves at the solver stage as expected. The first major obstacle materialized itself even before a single iteration of solver runtime was passed. This was a consequence of poor mesh quality for the purposes of an electrolyzer model. In the case of an electrolyzer where existing dimensions can be as low a scale of a unit as micrometres, see Table 1, the division of cells has to be very small in order for the solver to be able to even start the iterative solving process. Other complications found during meshing stage were the meshing of porous medium.

Specifically, the meshing of gas diffusion layers provided to be an important component of the mesh in order to prevent divergence in the solution. It was discovered that it is more a favourable practise to mesh the gas diffusion layers as structured as possible, as having large gradients near contact surfaces between porous and non-porous media can increase the solution divergence in the solver, sometimes even preventing the solver to solve even one iteration of equations. As displayed in Figure 11: it is recommended to direct inflation layers towards the catalysts, since the majority of the reactions take place at these layers. Additionally, the catalysts tend to be the smallest components of the entire cell, which necessitates more grid cells. With a simple geometry of a rectangular PEM-electrolyzer cell, a structured grid was both the preferable option, and easier to construct when compared to a more unstructured polyhedral-based grid.

From the solver settings, it is recommended to use first order “upwind” discretization schemes to discretize the fluid domain in electrolyzer cells. While second order “upwind” schemes can offer more accurate spatial accuracy by including more datapoints to the scheme, in the case of porous regions it can cause major instabilities for the governing equations when solving the fluid flow through them. It is also recommended to initialize the fluid flow problem using the standard method, by specifying the initial values manually. In the present model, gauge pressure and temperature were set same as their boundary condition equivalents, and the liquid water phase volume fraction was set to 1 in the SIMPLE simulations. For the coupled scheme, it is important to initialize the fluid flow from the anode side inlet, and with the liquid water phase volume fraction set to 0. This increases the solver runtime and the number of simulations required to reach convergence. However, if one were to initialize the coupled scheme with the same volume fraction as in the SIMPLE simulations, the software would estimate the hydrogen phase volume fraction wrong. An example and comparison between the initialization methods can be seen from Figure 32:

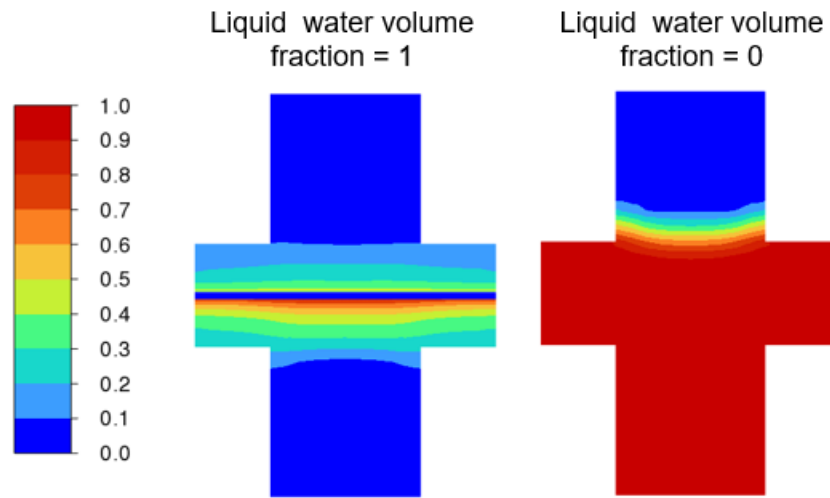


Figure 32. Comparison of hydrogen phase volume fractions in the Coupled scheme simulations for 1,746 V with two initialization methods.

The rest of the quantities to-be-initialized were set as their default values, or zero. From the solution controls, the relaxation factors were changed for momentum to be 0,3 and for the volume fraction to be 0,5, which were discovered to increase stability and provide faster convergence times for the solution.

The main validation method to determine if the charge transfer had converged was to include monitors of volumetric transfer current, which were taken as volume integrals over the catalyst layers. If both catalysts yielded the identical transfer current value, charge transfer was considered converged. It should be noted that charge transfer converged significantly faster than the governing equations. Another method of verifying the charge transfer was to plot a contour of electric potential for the mixture phase. Cathode side should display values of 0, and anode side should display values for the user-specified total voltage of the cell. An example of the electric potential contour can be seen from Figure 33:

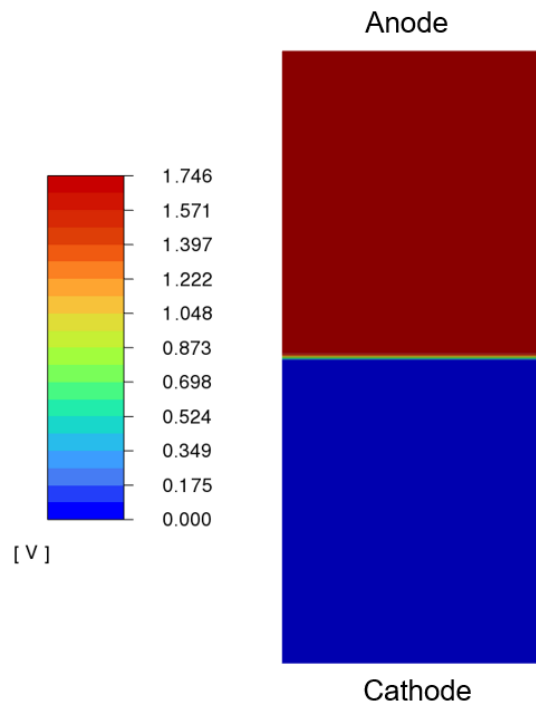


Figure 33. Example of contours of electric potential for voltage of 1,746 V.

Most of the troubleshooting and debugging of the simulation model was done by simply referring to the electrochemistry equations. First initial results yielded consistently lower values of current density, which indicated that the simulated cell was underperforming. By examining the equations for the transfer currents, see Equations (26) and (27), it was determined that the cathode side user specified reference current density j_c^{ref} was not enough, and was increased from 200 A/m² to 1500 A/m². The value was determined by simulating the cell at a constant voltage, and the resulting current density was compared to the measured data. It should be noted that the reference current density was not discussed by either Debe et al. (2012) or Toghyani et al. (2018) in their respective papers.

6 Conclusions

The main goals of the thesis were set to be the investigation of academic literature for the current status of CFD modelling of electrolyzers, and the simulation of a three-dimensional PEM-electrolyzer with all associated physics. It can be concluded that both goals were passed with adequate results.

From the literature review it was discovered that modelling methodologies varied across multiple different research papers. This variance was mostly caused by the simplifications used in the studies, which included two-dimensional cases, isothermal cases, and more. It was also discovered from literature that despite the simplifications, many papers found success and good agreement between the simulation results and experimental data. However, it should be noted that almost universally the experimental data used for result validation was performance data in the form of polarization curves.

The CFD simulations conducted in the thesis included multiphase flow, heat transfer, turbulence, and electrochemistry, i.e., species and charge transfer. The results were compared against performance measurement data provided by Debe et al. (2012) and were discovered to be in satisfactory agreement. The only discrepancies between the simulation results and measured data were found at the lowest values of voltage, which was a common phenomenon in many other research papers on the topic. Current density of the simulated electrolyzer cell was at the highest voltage measured to be $1,16 \text{ A/cm}^2$, and $0,005 \text{ A/cm}^2$ at the lowest value of voltage. The performance of the cell was visualized with the contour plots of hydrogen mixture volume fraction and velocity, where the development of hydrogen production was clearly more present and evenly distributed across the cell with the higher voltages. This was also displayed in the mass flow rates of the hydrogen mixture phase at the cathode side outlet. The velocity plots in particular display how the fluid flow in the cathode side of the electrolyzer begins to form when the total voltage of the cell is increased. Additional simulations were conducted for the electrolyzer cell where membrane thickness of the cell was varied from $30 \mu\text{m}$ to $200 \mu\text{m}$. It was discovered that the $30 \mu\text{m}$ membrane increased the performance of the electrolyzer cell, and the membranes thicker than $50 \mu\text{m}$ began to underperform due to the increased ohmic losses of the cell. For reference, for the

highest voltage produced current density of 1,40 A/cm² with the 30 μm membrane, and 0,78 A/cm² and 0,46 A/cm² with the 100 μm and 300 μm thick membranes respectively.

Despite the adequate accuracy of the polarization curves produced in the simulations, the hydrodynamic results of the electrolysis cell have not been validated against measured data. The present methodology would without a doubt benefit from additional measurements, with quantities such as total hydrogen flow rate on the cathode side alongside temperatures and pressure levels within the cell. Between the two used pressure-velocity coupling schemes, the SIMPLE offered more simplified simulation process, and faster convergence times. However, turbulence was not able to be modeled with the scheme. By comparison the Coupled scheme offered more stable, more robust convergence and possibility to include turbulence with the cost of additional computational time, and less automated simulation process. The scheme also requires more intricate initialization methods than the SIMPLE scheme. Despite the downsides, the Coupled pressure-velocity coupling is still recommended for any future simulations as the scheme of choice.

A natural continuation of the work presented in the thesis would be to simulate a larger electrolyzer cell with more complicated geometry, such as serpentine or even concave. This would allow the methodology to be tested in a more industrial environment. This would also entail a larger mesh, which would require more much more computational time to solve. Additionally, complex geometries can cause problems during the meshing stage of simulations, where much care needs to be taken when meshing the porous components of the electrolyzer. An example model of a more complicated geometry can be seen from Figure 34:

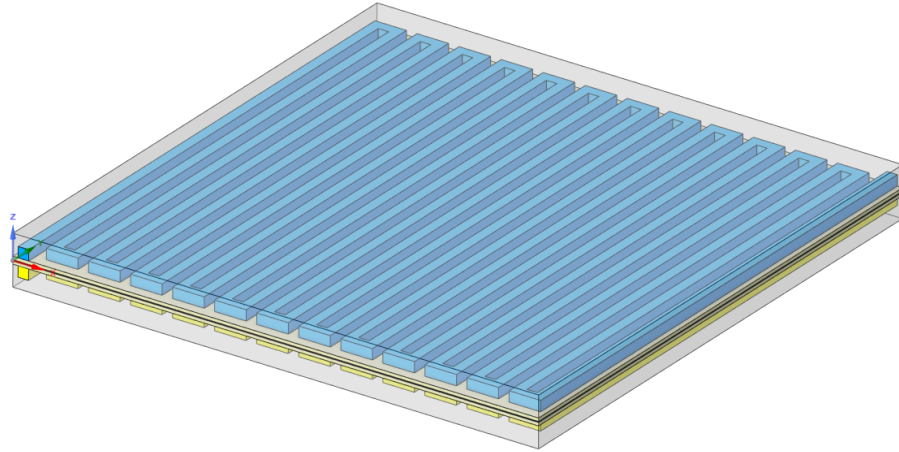


Figure 34. Example of a serpentine flow field electrolyzer cell.

For the present methodology a time dependent or transient simulation could also be tested to gain further insights as to how the development of hydrogen is affected by time. Another potential continuation for the thesis would be to attempt to simulate a PEM-fuel cell with the same properties and geometry, to study how well the present model would generate electricity and liquid water.

One can conclude from the results received from the simulation that the software used, ANSYS® Fluent, is capable when simulating PEM-electrolyzers with adequate accuracy, even without implementing any additional UDFs. Therefore, further model developments can be performed with relative ease, and the methodology applied in this thesis can be recreated without additional code to the solver.

References

ANSYS. 2023. *Ansys Fluent Theory Guide*. ANSYS Inc. [Online document].

Bessarabov, D., Wang, H., Li, H., Zhao, N. 2015. *PEM Electrolysis for Hydrogen Production: Principles and Applications*. Boca Raton: CRC Press. p. 2-8, 17-23, ISBN: 978-1-482-25232-3.

Chandesris, M., Médeau, V., Guillet, N., Chelghoum, S., Thoby, D., Fouda-Onana, F. 2015. *Membrane degradation in PEM water electrolyzer: Numerical modeling and experimental evidence of the influence of temperature and current density*. International journal of hydrogen energy. Vol. 40, Issue 3. p. 1353–1366.

Debe, M. K., Hendricks, S. M., Vernstrom, G. D., Meyers, M., Brostrom, M., Stephens, M., Chan, Q., Willey, J., Hamden, M., Mittelsteadt, C. K., Capuano, C. B., Ayers, K. E., Anderson, E. B. 2012. *Initial Performance and Durability of Ultra-Low Loaded NSTF Electrodes for PEM Electrolyzers*. Journal of the Electrochemical Society. Vol. 159, Issue 6. p. K165–K176.

El-Askary, W.A., Sakr, I.M., Ibrahim, K.A., Balabel, A. 2015. *Hydrodynamics characteristics of hydrogen evolution process through electrolysis: Numerical and experimental studies*. Energy (Oxford). Vol. 90, Part 1. p. 722–737.

Han, B., Mo, J., Kang, Z., Yang, G., Barnhill, W., Zhang, F.Y. 2017. *Modeling of two-phase transport in proton exchange membrane electrolyzer cells for hydrogen energy*. International journal of hydrogen energy. Vol. 42, Issue 7. p. 4478–4489.

Ho, T. X., Kosinski, P., Hoffmann, A. C., Vik, A. 2010. *Transport, chemical and electrochemical processes in a planar solid oxide fuel cell: Detailed three-dimensional modeling*. Journal of power sources. Vol. 195, Issue 19. p. 6764–6773.

IEA, 2022a., *Global Hydrogen Review 2022*, International Energy Agency. Paris. Available at: [Global Hydrogen Review-2022](#)

IEA, 2022b, *Renewables 2022*. International Energy Agency. Paris. Available at: [Renewables-2022](#)

IEA, 2023. *World Energy Outlook 2023*. International Energy Agency. Paris. Available at: [World Energy Outlook-2023](#)

Incropera, F.P., Dewitt, D.P., Bergman, T.L., Lavine, A.S. 2011. *Incropera's Principles of Heat and Mass Transfer*. Global edition. Singapore: WILEY. p. 933. ISBN: 978-1-119-38291-1.

Jensen, S. H., Sun, X., Ebbesen, S. D., Chen, M. 2016. *Pressurized Operation of a Planar Solid Oxide Cell Stack*. Fuel cells (Weinheim an der Bergstrasse, Germany). Vol. 16, Issue 2. p. 205–218.

Lee, J., Alam, A., Ju, H. 2021. *Multidimensional and transient modeling of an alkaline water electrolysis cell*. International journal of hydrogen energy. Vol. 46, Issue 26, p. 13678–13690.

Li, A., Song, C., Lin, Z. 2017. *A multiphysics fully coupled modeling tool for the design and operation analysis of planar solid oxide fuel cell stacks*. Applied energy. Vol. 190. p. 1234–1244.

Menon, V., Banerjee, A., Dailly, J., Deutschmann, O. 2015. *Numerical analysis of mass and heat transport in proton-conducting SOFCs with direct internal reforming*. Applied energy. Vol. 149. p. 161–175.

Ni, M., Leung, M. K. H., Leung, D. Y. C. 2007. *Parametric study of solid oxide steam electrolyzer for hydrogen production*. International journal of hydrogen energy. Vol. 32, Issue 13. p. 2305–2313.

Ojong, E. T., Kwan, J. T. H., Nouri-Khorasani, A., Bonakdarpour, A., Wilkinson, D. P., Smolinka, T. 2017. *Development of an experimentally validated semi-empirical fully-coupled performance model of a PEM electrolysis cell with a 3-D structured porous transport layer*. International journal of hydrogen energy. Vol. 42, Issue 41. p. 25831–25847.

Qian, X., Kim, K., Jung, S. 2022. *Multiphase, multidimensional modeling of proton exchange membrane water electrolyzer*. Energy conversion and management. Vol. 268. p. 116070–.

Riegel, H., Mitrovic, J., Stephan, K. 1998. *Role of mass transfer on hydrogen evolution in aqueous media*. Journal of applied electrochemistry. Vol. 28, Issue 1, p. 10–17.

Rivera, F. F., Pérez, T., Castañeda, L. F., Nava, J. L. 2021. *Mathematical modeling and simulation of electrochemical reactors: A critical review*. Chemical engineering science. Vol. 239. p. 116622–.

Rizvandi, O. B. & Frandsen, H. L. (2023) *Modeling of single- and double-sided high-pressure operation of solid oxide electrolysis stacks*. International journal of hydrogen energy. Vol. 48, Issue 77. p. 30102-30119.

Sandoval, M. A., Fuentes, R., Pérez, T., Walsh, F. C., Nava, J. L., Ponce de León, C. 2021. *Modelling and simulation of H₂-H₂O bubbly flow through a stack of three cells in a pre-pilot filter press electrocoagulation reactor*. Separation and purification technology. Vol. 261. p. 118235–.

Schalenbach, M., Tjarks, G., Carmo, M., Lueke, W., Mueller, M., Stolten, D. 2016. *Acidic or Alkaline? Towards a New Perspective on the Efficiency of Water Electrolysis*. Journal of the Electrochemical Society. Vol. 163, Issue 11. p. F3197–F3208.

Schillings, J., Doche, O., Deseure, J. 2015. *Modeling of electrochemically generated bubbly flow under buoyancy-driven and forced convection*. International journal of heat and mass transfer. Vol. 85. p. 292–299.

Toghyani, S., Afshari, E., Baniasadi, E., Atyabi, S.A., Naterer, G.F. 2018. *Thermal and electrochemical performance assessment of a high temperature PEM electrolyzer*. Energy (Oxford). Vol. 152 p. 237–246.

Vachaparambil, K. J. & Einarsrud, K. E. .2021. *Numerical simulation of continuum scale electro-chemical hydrogen bubble evolution*. Applied Mathematical Modelling. Vol. 98, p. 343–.

Amores, V. E., Ruiz, J. R., Rodríguez, C. M., Escribano, P. G. 2011. *Study of an alkaline electrolyzer powered by renewable energy*. In: Excerpt from the Proceedings of the 2011 COMSOL Conference in (Stuttgart). [Online]. Available at ResearchGate: [Study of an Alkaline Electrolyzer Powered by Renewable Energy](#)

Versteeg, H. K. & Malalasekera, W. 2007. *An introduction to computational fluid dynamics: the finite volume method*. 2nd ed. Harlow: Pearson/Prentice Hall. p. 24. ISBN: 978-0-13-127498-3

Wang, T., Wang, J., Wang, P., Wang, F., Liu, L., Guo, H. 2023. *Non-uniform liquid flow distribution in an alkaline water electrolyzer with concave-convex bipolar plate (CCBP): A numerical study*. International journal of hydrogen energy. Vol. 48, Issue 33, p. 12200–12214.

Wilcox, D. C. 2006. *Turbulence modeling for CFD*. 3rd edition. La Cañada (CA): DCW Industries. p. 26-27, 40, 107, 128. ISBN: 978-1-928729-08-2.

White, F.M. 1998. *Fluid Mechanics*. 4th edition. McGraw-Hill. p. 24, 348-349, 367. ISBN: 978-0-072281-92-7

Xiang, C., Papadantonakis, K. M., Lewis, N. S. 2016. *Principles and implementations of electrolysis systems for water splitting*. Materials horizons. Vol. 3, Issue 3, p. 169–173.

Zarghami, A., Deen, N. G., Vreman, A. W. 2020. *CFD modeling of multiphase flow in an alkaline water electrolyzer*. Chemical engineering science. Vol. 227. p. 115926–.

Zhang, Z. & Xing, X. 2020. *Simulation and experiment of heat and mass transfer in a proton exchange membrane electrolysis cell*. International journal of hydrogen energy. Vol. 45, Issue 39, p. 20184–20193.